# IMPROVING JOINING PERFORMANCE OF COMPOSITES BY ELECTRO-SPINNING OF NANO FIBERS

**A Thesis Submitted to**
**the Graduate School of**
**İzmir Institute of Technology**
**in Partial Fulfillment of the Requirements for the Degree of**

**MASTER OF SCIENCE**

**in Mechanical Engineering**

**by**
**Gözde ESENOĞLU**

**December 2021**
**İZMİR**

*Dedicated to my family.*

# ACKNOWLEDGMENTS

I would like to give my sincere thanks to my advisor, Prof. Metin TANOĞLU for his guidance, support, motivation, and encouragement during my thesis. Also, I would like to thank the thesis jury members for their interest.

Besides, this dissertation was supported by Tubitak project number 218M801. I would like to thank the rest of my Tubitak project committee members Assoc. Prof. Engin AKTAŞ and Assoc. Prof. Murat BARIŞIK for their encouragement and constructive comments.

Also, I would like to thank Turkish Aerospace Industries Inc. (TUSAŞ) of Turkey for providing film adhesive, unidirectional and woven carbon prepregs.

And also, I would like to thank IZTECH Center for Materials Research (MAM) for their contribution to the analysis in this thesis.

My laboratory friends who helped and supported me throughout my Master's Education; I would like to thank Melisa YEKE, Nazife ÇERÇİ, Ceren TÜRKDOĞAN, Zeynep AY, Hande İPLİKÇİ, Mehmet Deniz GÜNEŞ, Osman KARTAV, Seçkin MARTİN and Yusufcan UZ.

Finally, and most importantly, I dedicate this thesis to my beloved family for their love, patience and support throughout my life. I would like to thank my dear father Namık ESENOĞLU, my dear mother Aysun ESENOĞLU and my dear little sister Dr. Gökçe ESENOĞLU for everything. My dear family, I am grateful to you for raising me to be a free and good individual in every sense. I will always make you proud.

# ABSTRACT


## IMPROVING JOINING PERFORMANCE OF COMPOSITES BY ELECTRO-SPINNING OF NANO FIBERS

Mechanical joints (screws, rivets, etc.) traditionally used in composite materials (screws, rivets, etc.) increase weight and act as a stress collector, causing serious delamination problems. On the other hand, development of alternative joining techniques has become an important alternative in the composite industry due to their sensitivity to corrosion, electromagnetic properties/radar absorption properties, labor cost, and adverse effects on the manufacturing process.

In this thesis, the effects polyamide 66 (PA 66) nanofiber coatings, applied on two different prepreg systems (UD and woven) on the mechanical properties of the joint region were investigated. Moreover, the microstructures of the produced PA66 nanofibers were investigated. The produced nanofibers were directly coated on the bond zone layer (top surface) of the carbon prepregs. The reference and nanofiber coated prepregs were laminated and cured using hot pressing method, and then the laminated layers were joined together using with the secondary bonding method employing FM300K film adhesive under a hot press. Tensile, compression, bending, shear, charpy-impact and double cantilever beam (DCB) tests were performed on the produced samples. The effect of homogeneity and areal weight density (AWD) of PA66 nanofibers on mechanical performance of the composite specimens was investigated. The morphology and post-test deformations of the nanofibers were investigated by scanning electron microscopy (SEM). The thermal properties of PA66 nanofibers were investigated by the differential scanning calorimetry (DSC) method. By comparing the SEM images and the lap shear test results, the most efficient parameters for the mechanical performance of the composites were determined. The results showed that PA66 nanofibers produced with a 10% wt solution ratio and 10 min coating time were the most effective on joining of the composites. The incorporation of PA66 nanofibers produced with the electro-spinning tecnique over the joining region of the composite plates has been proven to increase the joining region performance of the composite parts.

# ÖZET

## NANO ELYAFLARIN ELEKTRO-EĞİRİLMESİ İLE KOMPOZİTLERİN BİRLEŞME PERFORMANSININ İYİLEŞTİRİLMESİ

Kompozit malzemelerde geleneksel olarak kullanılan mekanik mafsallar (vidalar, perçinler vb.) sadece ağırlığı artırmakla kalmaz, aynı zamanda stres toplayıcı olarak da etki ederek ciddi delaminasyon sorunlarına neden olur. Aynı zamanda korozyona karşı hassaslığı, elektromanyetik özellikleri/radar absorpsiyon özellikleri, işçilik maliyetini ve imalat sürecini olumsuz etkilemesi nedeniyle alternatif birleştirme tekniklerinin geliştirilmesi kompozit sektöründe önemli bir konu haline gelmiştir.

Bu tezde, poliamid 66 (PA 66) nanoliflerin iki farklı prepreg (UD ve dokuma prepreg kumaşlar) yüzeyine kaplanması sonucu birleşme bölgesi mekanik özellikleri üzerindeki etkileri incelenmiştir. Ayrıca üretilen PA66 nanoliflerin mikroyapıları araştırılmıştır. Üretilen nanolifler doğrudan karbon prepreglerin birleşme bölgesi katmanı (üst yüzey) üzerine kaplanmıştır. Referans ve nanofiber katkılı prepregler laminasyon sonrası sıcak pres yöntemiyle kürlendi ve ardından sıcak preste FM300K film yapıştırıcı kullanılarak ikincil bağlama yöntemiyle birleştirilmiştir. Üretilen numuneler üzerinde çekme, basma, eğilme, kesme, charpy-darbe ve çift konsol kiriş testleri (DCB) testleri yapılmıştır. PA66 nanoliflerinin homojenliğinin ve alan yoğunluğunun mekanik performansa etkisi araştırılmıştır. Nanoliflerin morfolojisi ve test sonrası deformasyonları taramalı elektron mikroskobu (SEM) ile incelenmiştir. PA66 nanoliflerinin termal özellikleri Diferansiyel Taramalı Kalorimetri (DSC) yöntemi ile araştırılmıştır. SEM görüntüleri ve bindirme kesme testi sonuçları karşılaştırılarak kompozitlerin mekanik performansı için en verimli parametreler belirlenmiştir. Sonuçlar, ağırlıkça %10 çözelti oranı ve 10 dakikalık kaplama süresi ile üretilen PA66 nanoliflerinin kompozitler üzerinde en verimli olduğunu göstermiştir. Elektro-eğirme tekniği ile birleştirme bölgesine PA66 nanofiberlerin eklenmesi sonucu kompozit levhaların birleşme bölgesi performansınınarttığı ölçülmüştür.

# TABLE OF CONTENTS

# LIST OF FIGURES

**Figure** **Page**

**Figure** **Page**

# LIST OF TABLES

# LIST OF SYMBOLS AND ABBREVIATIONS

| | |
|---|---|
| R | rate of crosshead motion, mm [in.]/min |
| L | support span, mm [in.] |
| d | depth of beam, mm [in.] |
| Z | rate of straining of the outer fiber, [in./ in./min] |
| s | stress in the outer fibers at midpoint, MPa [psi] |
| P | load N [lbf] |
| b | width, mm [in.] |
| $\varepsilon_f$ | strain in the outer surface, mm/mm [in./in.], |
| D | maximum deflection of the center of the beam, mm [in.] |
| $E_B$ | modulus of elasticity in bending, MPa [psi] |
| m | slope of the tangent N/mm [lbf/in.] |
| L' | half width of loading block. |
| F | large displacement correction factor. |
| N | loading block correction factor. |
| $\sigma_f$ | flexural strength [$N/mm^2$] |
| t | distance from the loading block pin to the centerline of the upper sample arm. |
| $\|\Delta\|$ | effective delamination extension to correct for rotation of DCB arms at delamination front. |
| $\alpha$ | delamination length. |
| $\delta$ | load point deflection. |
| GI | opening Mode I interlaminar fracture toughness. |
| PA66 | polyamide 6,6 |
| PAN | polyacrylonitrile |
| DCB | double cantilever beam |
| DSC | differential scanning calorimetry |
| CF/EP/PA66 | carbon fiber reinforced epoxy matrix modified with PA66 |
| CNT | carbon nanotube |
| UD | unidirectional |
| AWD | areal weight density |

# CHAPTER 1

# INTRODUCTION

## 1.1. Defination of Composite Materials

Composite materials consist of a macro-level combination of at least two different materials with superior properties. Composite materials have been used since ancient times. Many civilizations in the history of the world have developed building materials to use in daily life by combining materials found in nature. For example, bricks were produced by mixing mud and straw in certain proportions. Thus, the story of using composites began. With the latest technological developments, the interest in quality and innovative materials is increasing. For this reason, composite materials have developed a little more every day. In composite materials, matrix resin properties, type of reinforcement material and placement method can increase the mechanical, chemical and thermal properties of the composite, making composites very different from conventional materials. These superior properties such as high specific strength and elastic modulus, low density, long life, cheaper, lighter and high corrosion resistance have made composites a serious competitor for other traditional engineering materials such as steel, aluminum, titanium alloys. For example, by replacing stainless steel with fiber-reinforced polymer composites, a 60-80% reduction in the weight of the material has been observed. In addition, reducing fuel consumption with the use of composite materials has become popular in the aircraft, automobile and marine industries.

**(cont. on next page)**

Figure 1.1. Example view of some structural applications of composites.

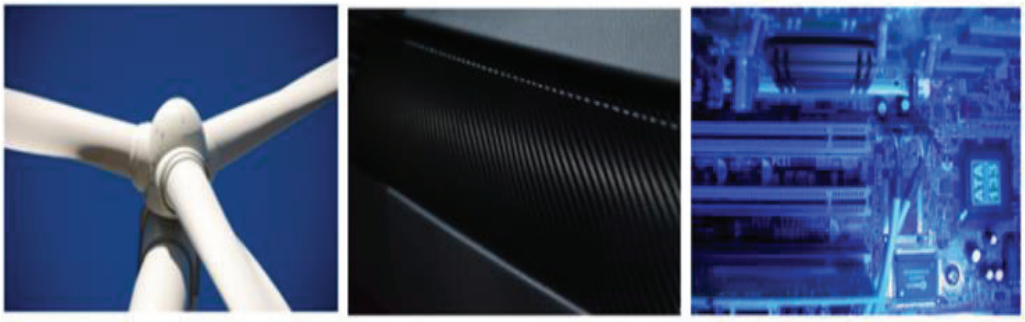

Figure 1.1. (cont.)

There are various type advanced composite materials such as reinforced plastics such as carbon-fiber-reinforced polymer or glass fiber, ceramic and metal matrix composites. Different types of fibers such as glass, carbon, aramid have been used in industry. While carbon fibers are used as the main reinforcement material in the aviation industry, glass fiber reinforced composites are commonly used in the automotive industry. However, composite materials still lag behind glass fiber (85%), but the use of carbon fiberhas become more common recently. About 75% of the carbon fibers are reinforced with epoxy matrices. In addition, carbon fiber reinforced composites have a wide range of applications from aviation and space to automobiles, from sports equipment to health equipment. In addition, due to its light, durable and strong features, it has a very important use in military vehicles. For example, newly produced airplanes today are largely made of composite materials. Most of the Airbus A380 fuselage, wing and stabilizer parts are manufactured using prepreg composites. Figure 1.2 shows the fuselage and composite structures of the aircraft, which consists of 55% composite parts.

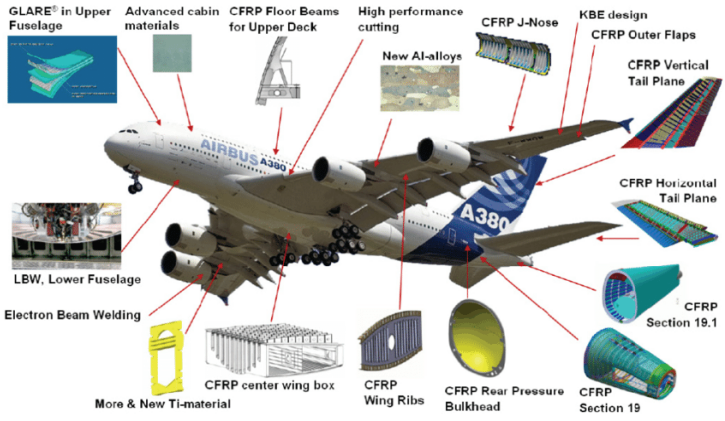


Figure 1.2. The AIRBUS A380 aircraft composite applications

(Source: www.airbus.com).

## 1.2. Manufacturing techniques for prepreg based composites

There are numerous methods for producing lamina from composite components. Figure 1.3 shows the techniques used to fabricate composite structures. In this thesis, the hot press technique (compression molding) is used in the production of carbon fiber reinforced / epoxy composite prepreg plates.

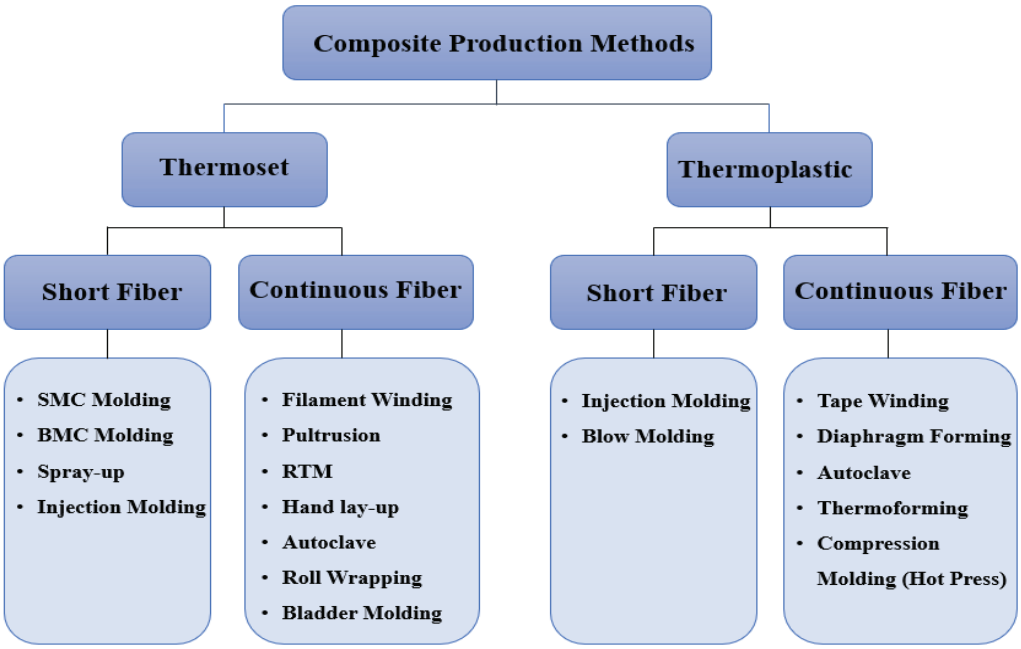


Figure 1.3. Composite manufacturing techniques

A hot press is a method used to produce flat plates of constant thickness by compression molding of the composite placed in an open and heated device. Also, the hot press technique is widely used in automotive, aerospace and other industrial practices [1]. The shape, size and fiber angle of the prepregs are determined and cut according to the places to be used and their requirements. The cut prepregs are laid to cover the entire surface of the mold [2]. Before the prepregs are laid in the hot press mold, Kapton film, on which gel (frecote) is applied, is placed on the mold surface so that the part can be easily removed from the mold and the surface is smooth. Press is closed after a certain pressure setting is made and pressure is continued until the material is cured, then after the mold cools down, the pressure is pulled over the plate and the plate is taken from the mold (Figure 1.4). The dies used for this pressing process are made of stainless steel or

aluminum. The molds are quite simple as mostly laminates are made using this technique. Mold design for the hot press process is simpler compared to other mold production methods. In the hot press method, there is no injection material to be sent to the mold. Therefore, there is no need for a runner in this method. The most important parameter for the hot press method is the same thermal expansion coefficient between the mold material and the composite structure. The advantages of the method are as follows [3];

- A one-step method,
- Fast curing times and short cycle times,
- Reduced tool investment (compared to metal forming processes),
- Suitable for mass production.

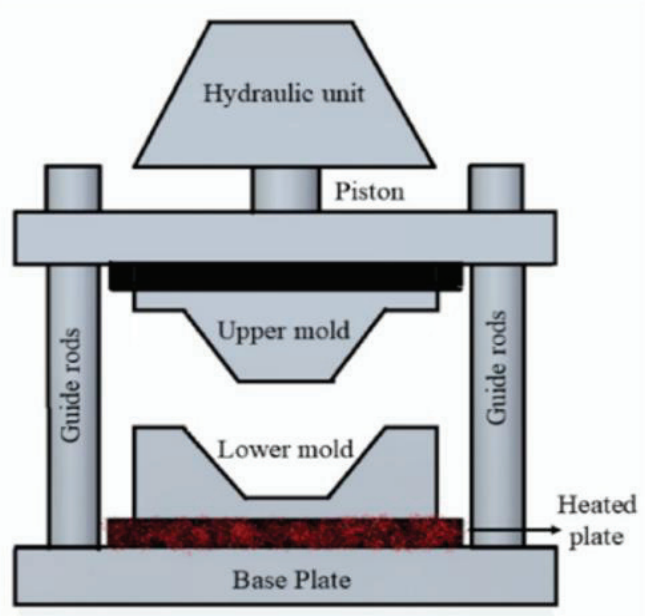


Figure 1.4. Schematic of the hot press technique
(Source:Rangaswamy et al., 2021 [3])

## 1.3. Combination and Improvement Methods for Structural Composite Parts

### 1.3.1. Co-curing, Co-bonding and Secondary Bonding

The use of adhesives for joining composite structures is increasing day by day due to its superior properties such as high bond strength, improved stress distribution and

joining multi-material mixed structures [4]. In addition, adhesive bonding allows structures to be repaired using small composite parts, and these repairs can be made without much damage to the part [5]. The adhesive bonding method provides a continuous and considerably larger bonding area, which significantly reduces the stress intensity compared to mechanical fasteners. However, it should be noted that stress concentrations are still present in the adhesive and bonded materials due to the natural discontinuity of the materials in the bonding zone. It has been proven that the highest stresses in materials occur mostly around the joint zone [6]. The stresses in the adhesive and on the bonded surfaces are divided into two as shear stress and peel stress according to the type of movement. For adhesive joints used to join developed composite materials, the peel stress is applied directly in the direction of the weak region of the matrix of the material, thus having a very significant effect on the bond strength. Often, the load-bearing ability of a composite structure is governed by the weakest stressed regions. Therefore, in the adhesive-bonded regions, the bond/adhesive interface relationship needs to be improved under certain load conditions. The surface improvement techniques used in the preparation of the adhesion zone and the suitability of these techniques for different materials were investigated [7,8]. This often provides the required interface strength between the adherent and the adhesive.

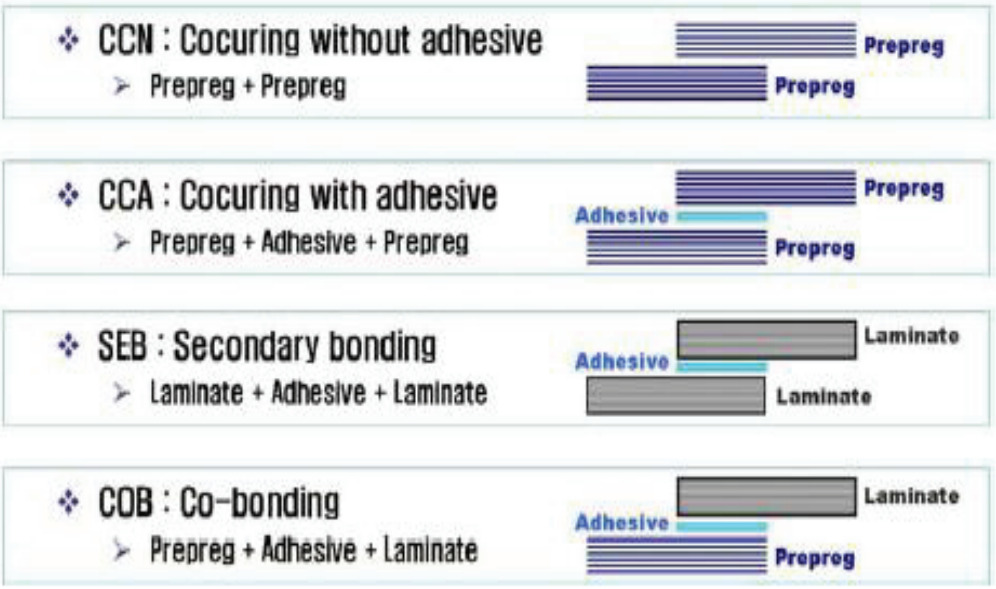


Figure 1.5. Schematic of the hot press technique

(Source:Rangaswamy et al., 2021[3])

Traditionally used mechanical fasteners such as screws and rivets not only increase weight but also act as a stress concentrator, impairing the structural capacity of components and causing severe delamination problems. Therefore, alternative bonding techniques for joining have become an important issue, especially in the aerospace industry. In recent years, studies on co-curing, co-bonding and secondary bonding methods have been carried out [9] These methods are shown schematically in Figure 1.5. In the co-curing method, the curing and bonding processes of two parts occur simultaneously. Among the important advantages of the co-curing method are; large and complex structures can be produced in a single curing cycle. Thus, labor costs and energy consumption can be reduced, production can be accelerated, and the integration and stability of the part can be increased [10]. In the secondary bonding method, two pre-cured rigid adherents are joined using an adhesive. The co-bonding method is where uncured prepregs are joined to a rigid composite piece that has been pre-cured using either a liquid adhesive or a film adhesive [11].

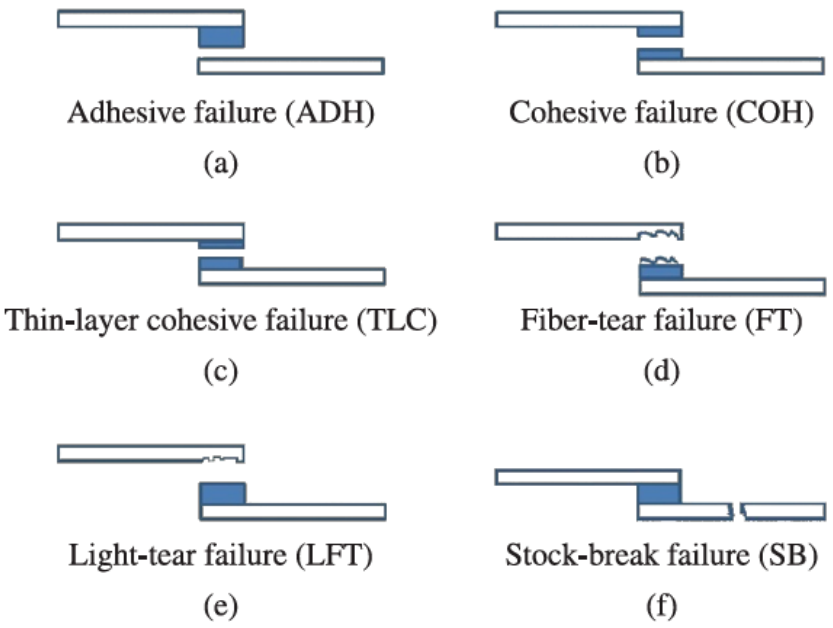


Figure 1.6. Representation of failure modes characteristic of adhesive joints submitted to shearing (Source: Quini and Marinucci, 2021[12]).

Generally, two different fracture mechanisms occur in materials bonded by bonding methods such as co-bonding, co-cure and secondary bonding. These fracture mechanisms are called cohesive and adhesive fractures. Adhesive breakage mechanisms are the failure of the material at the interface. These failures occur between the adhesive and one of the adhered ones. Generally, these failure mechanisms occur in bonded structures where adhesion is weak [13]. Figure 1.6, shows schematically the different types of failures in glued joints. The figure of adhesive and adhesive failure at adhesive-bonded joints shows, (a) adhesive failure, (b) cohesive failure, (c) thin-layer cohesive failure (d) fiber-tear failure, (e) light-tear failure and (f) stock-break failure [12]. De Freitas and Sinke 2014 proved that the failure modes of the adhesive that occurred in the samples joined using the adhesive were more important than the max load. They also showed that the surface treatment applied to the adherents is very important to obtain well-adhered surfaces.

## 1.3.2. Electrospinning Methods

Nanofiber production by electrospinning method is not a new technology. This method emerged when William Gilbert, while continuing his studies on magnetism, accidentally observed the effect of electromagnetism on liquids [15]. In his research, he noted that water moves in a cone shape from a dry surface to an electric field at a certain distance [15,16].

This system allows multiple types of polymers, fibers, and particles to be interconnected to produce nano sized sheets. The electrospinning system is used to produce nanofibers by subjecting the polymer solution to a certain voltage. In the electro-spinning process, the voltage value to be applied in the appropriate range is selected to neutralize the surface tension force of the polymer liquid. The polymer liquid jets formed by this applied voltage become solid and are sprayed towards a grounded collector. The liquid elongates along with the jet motion and collects as an interconnected net-like solid fibrous structure. Studies show that the voltage range required to produce nanofibers is between 5 and 30 kV [17].

Electrospinning is one of the most useful and productive methods for producing polymer-based nano fibers. Electrospinning is a multidisciplinary method that includes polymer chemistry, physics, fluid dynamics, electrical, mechanical and textile engineering. A classical electrospinning method (Figure 1.7) consists of a syringe pump, a high voltage source and a grounded metal retractor.

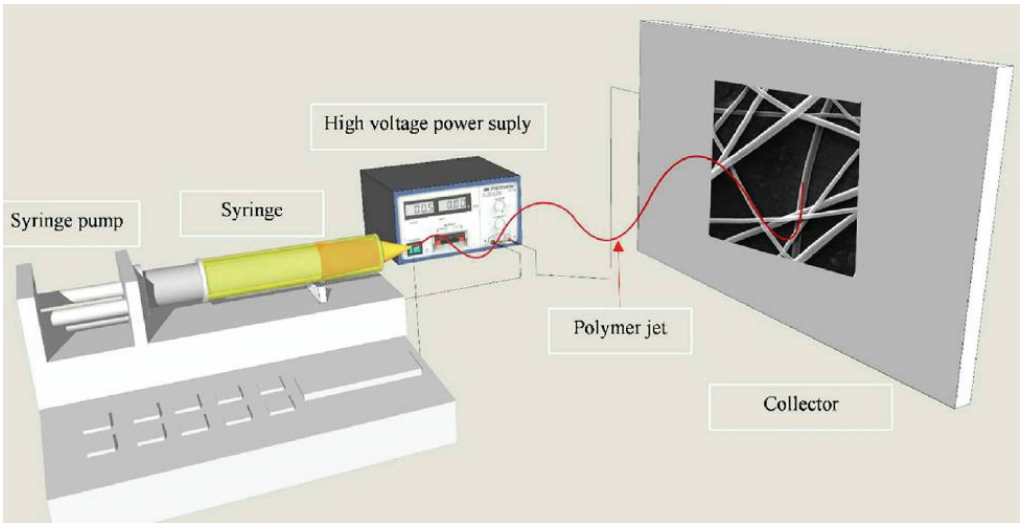


Figure 1.7. Schematic design of the basic set-up for the electrospinning process (Source: Rostamabadi et al., 2021[18]).

There are four basic components required for the process: a small diameter capillary tube, a syringe, a high voltage generator, and a metal collector. During the process, before the polymer liquid jet reaches the collector, the solution jet changes from liquid to solid and forms interconnected nano-sized fibers [19]. The electric field is subjected to the end of the capillary tube containing the solution liquid held by the surface tension. The mutual charge repulsion and accumulation of surface charges on the electrode cause the surface tension to create an opposite force [20]. As the effect of the electric field increases, the solution liquid sent from the tip of the needle takes the form of a hemisphere, which shows that the conical structure called the Taylor cone in the literature is formed (Figure 1.8).

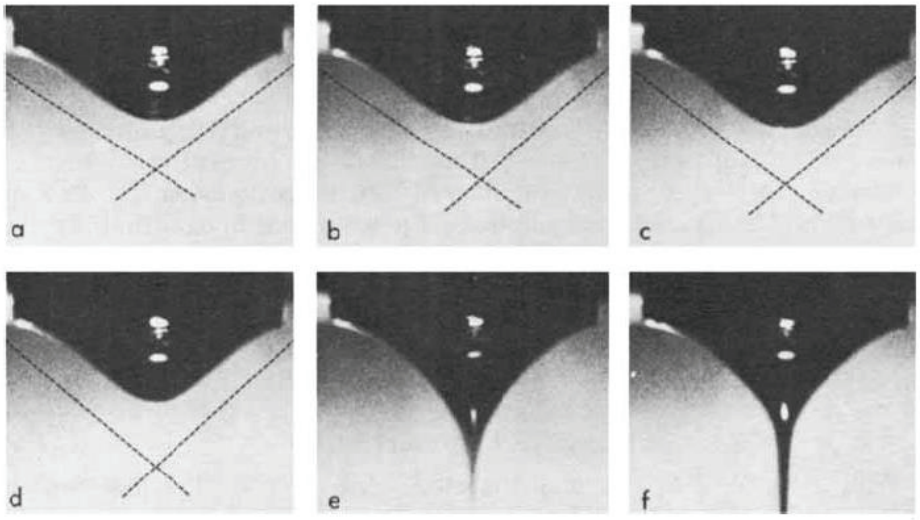


Figure 1.8. Taylor cone and jet formation with the increasing voltage effect by progressing drop on the tip of the needle (a) 110º (b) 107º (c) 104º (d) 100º (Source: Larrondo and Manley, 2021[21]).

The critical value at which the voltage-charged liquid jet is launched from the Taylor cone occurs when the electric field is increased and the repugnant electrostatic force surpasses the surface tension. The tension of the polymer-solvent liquid jet is released, allowing it to enter the irregularity and fiber elongation time. This causes the evaporating solvent jet to become long and thin nanofibers. The de-stressed jet goes into a melting state and changes from the liquid phase to the solid phase as it moves through the air.

Today, it is clearly stated in the literature that nanofibers with diameters up to 5nm from more than hundreds of polymers are produced successfully by the electrospinning method. The majority of polymers are dissolved in the solvent before electrospinning. For example, polymer pellets are added to the solvent prepared in a certain ratio, which is prepared in a glass container, and it is completely dissolved. The polymer solution is filled into the syringe to be electrospun and transferred to the capillary tube. Solution preparation and electrospinning are usually carried out at room temperature and under atmospheric conditions. In addition, some polymers may emit harmful or foul odors that may affect human health, so a room with ventilation systems should be preferred during processing. In addition, due to the presence of high voltage in the environment during the process, care should be taken not to touch the liquid jet and the collector. With the electrospinning method, it is possible to produce different nanofiber structures when a polymer is dissolved in different solutions or solution ratios (Figure 1.9).

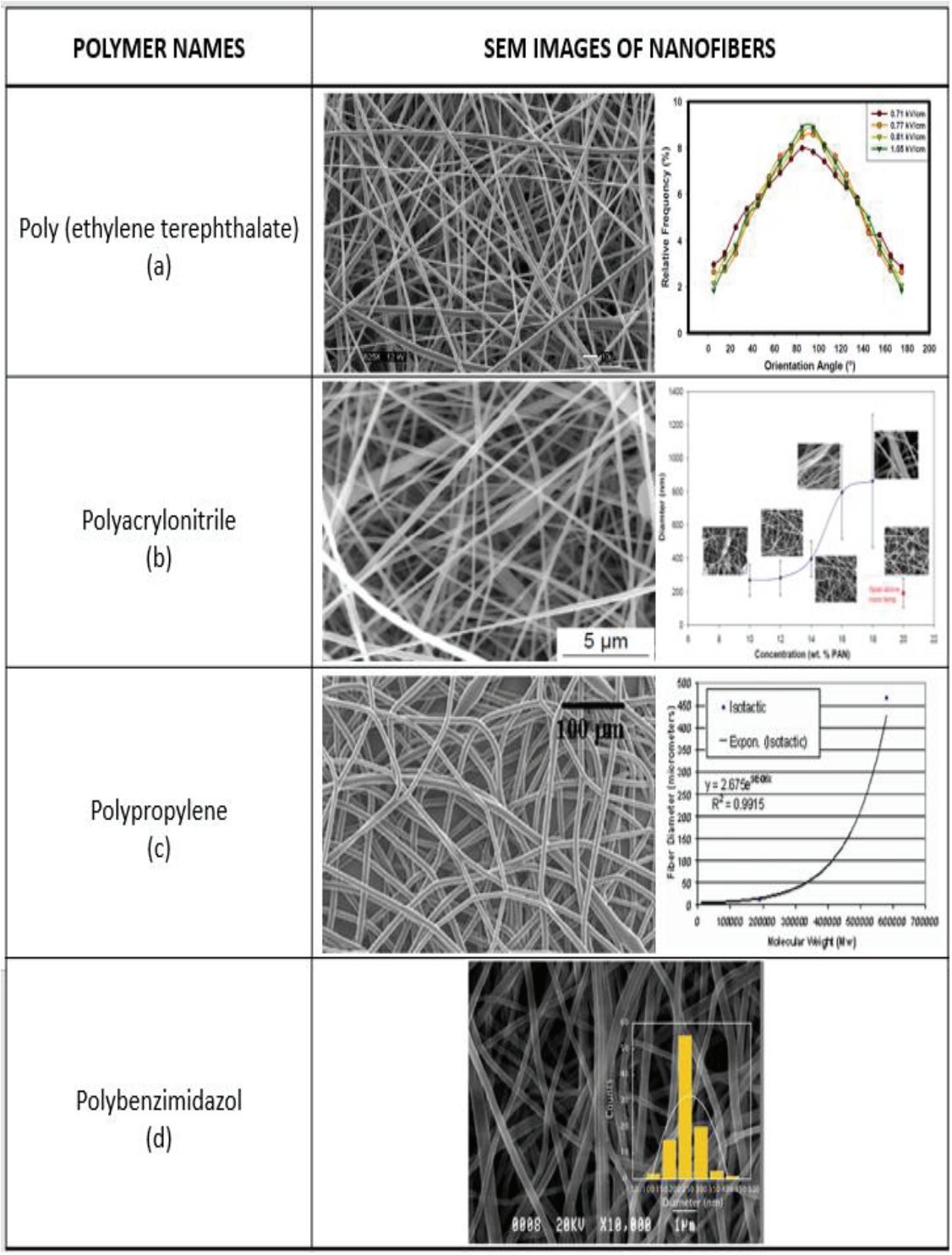


Figure 1.9. Some studies with nanofibers produced from a) Poly(ethylene terephthalate) [17], b) polyacrylonitrile [16], c) polypropylene [22] and d) polybenzimidazole [23] polymers (Source: Mohan 2002, Lam 2004, Lyons 2004, Kim 2004).

Numerous parameters affect the ability to obtain nanofibers from polymer liquid by the electrospinning method. These parameters are examined under three headings; solution properties such as viscosity, elasticity, conductivity and surface tension, etc., production properties such as hydrostatic pressure at the needle tip, potential difference and gap at the capillary tip (distance between the tip and the collecting screen), etc., and environmental properties such as polymer liquid temperature, humidity and room temperature, etc. The surface properties, morphology and structure of polymer nanofibers should be controlled (Figure 1.10). Many studies have been carried out to determine the fiber coating parameters of polymers by the electrospinning method. For example, polymer solutions must have high concentration and viscosity. However, the high viscosity and concentration of the polymer solution prevent fiber formation. Therefore, the determination of optimum parameters is vital to create the appropriate fiber structure. The charged density of the polymer liquid solution should be sufficiently high and the surface tension sufficiently low. In addition, some changes can be made to the fibers by reducing the distance between the needle tip and the nanofiber collector The structural properties of the fibers can be changed by the density of the fiber going to the collector, nozzle/collector distance and voltage [24].

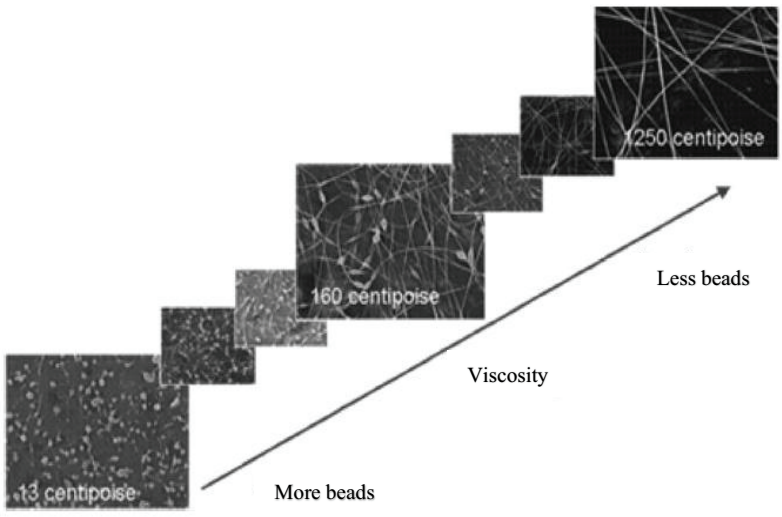


(a) viscosity - bead structure relationship

**(cont. on next page)**

Figure 1.10. (a) viscosity - bead structure relationship (b) concentration - bead structure relationship (c) voltage - bead structure relationship (Source: Lee et al., 2003[25])

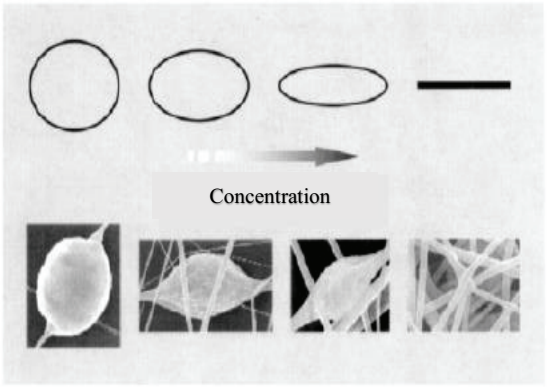


(b) concentration - bead structure relationship

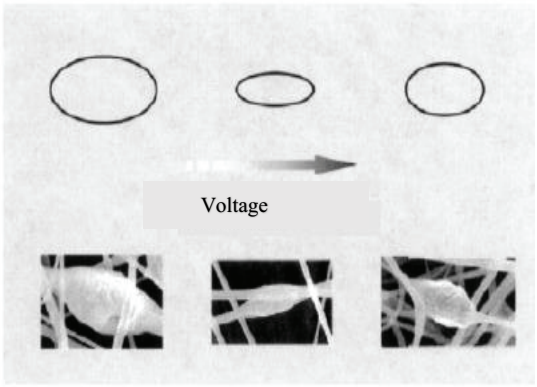


(c) voltage - bead structure relationship

Figure 1.10. (cont.)

## 1.4. Objectives

In this study, it was aimed to improve the joint area performance of structural fiber-reinforced composite parts joined by innovative methods used in the aircraft industry. In this way, it is aimed to prevent the disadvantages of mechanically joined parts (riveting-connector, etc.) on the structure, to increase their mechanical properties and fatigue life, and to reduce their weight. This study has an innovative approach on increasing the joint zone performance of composites by electrospinning method. In this study, 10 wt% PA 66 nanofibers were coated on the prepreg surface by electro-spinning to improve the performance of the joining area. To examine the mechanical performance of PA 66 nanofibers in the bonding zone, reference composite laminate samples and PA 66 interlayed composite laminate samples were produced using the hot press method. Lap-shear test, Charpy impact test and DCB tests were performed on the prepared samples. The thermal properties of the spun PA66 nanofibers were investigated by Differential Scanning Calorimetry (DSC) analysis. It was found that the shear strength, Mod-I fracture toughness and impact energy of CF/EP composites has been increased by 18.7, 10.38 and 153.15 %, respectively, with PA66 nanofibers integrated to the joint zone. Another important analysis is that the weight gain of nanofibers on composites is negligible. This is one of the most important features of the thermoplastic nanofiber interleaving method.

# CHAPTER 2

# LITERATURE SURVEY

The trend towards composite materials in the aviation industry is constantly increasing. This trend has contributed to the structurally higher performance of the aircraft, improving production processes and manufacturing time, and reducing operational risks [9]. The use of prepreg fabrics is increasing day by day in the production of high-performance structural composites used in aerospace applications. Prepregs are widely used in many sectors, especially in the aviation sector, due to the many advantages they provide. Some of these advantages are high corrosion resistance, high strength and better fatigue strength compared to metals and lower weight. Considering the problems encountered in traditional composite production (dry areas, inhomogeneous resin distribution, void formation, non-homogeneous curing and low-temperature curing, etc.), the use of prepregs has increased [26]. In addition to composite materials, alternative bonding techniques have become an important issue in the aviation industry. This is because conventionally used mechanical fasteners such as screws and rivets act as a stress absorber that not only adds weight but also degrades the structural capacity of components, causing severe delamination problems and corrosion, affecting and negatively affecting electromagnetic properties/radar absorption properties. Recently, studies have been focused on co-curing, co-bonding, and secondary bonding methods to eliminate the negative effects of conventional mechanical fasteners [9]. Song et al. 2010, produced single lap joint specimens using four different joining methods (Co-curing without adhesive, co-curing with adhesive, co-bonding and secondary bonding) in this study. They compared the effects of the joint method with the tests performed on the strength of the joint area. When the results were examined, it was determined that the highest strength was in the samples produced using the co-curing and secondary bonding methods, and the lowest strength was in the samples produced by the co-bonding method. These methods are shown schematically in Figure 2.1. In the co-curing method, the curing and bonding processes of two parts take place simultaneously. Mohan et al. 2015, investigated the mixed-mode fracture toughness by adding alumina nanoparticles and electrospun nanofibers to the joint cured and two secondary bonded composite bond

systems. According to the test results, cohesive breakage was reported in samples joined by secondary bonding, and adhesive breakage was reported in samples joined by the co-curing method. In addition, as a result of the tests performed for each sample, it was determined that the mode II fracture toughness was above the mode I fracture toughness.

Recently, it has been studied to improve the Mod-I fracture toughness value by adding nanofils to the resin. However, it is one of the difficulties to ensure the homogeneous distribution of these fillers in the resin. The extreme increase in the viscosity of the resin with the addition of fillers is a major problem for composite production techniques other than autoclaves, such as resin transfer molding and vacuum infusion. Therefore, some researchers have worked to improve the technique of interleaving a thermoplastic or thermoset material in the interlayer region [29]. Van der Heijden et al.(2014), reported an approximately 100% improvement in initial interlayer fracture toughness by sprinkle a 20 g/m$^2$ polycaprolactone (PCL) nanofiber into the interlayers of resin transfer molded glass fiber epoxy laminates. Saz-orozco, Ray, and Stanley (2015) investigated the Mode I fracture toughness of glass fiber/vinyl ester (GF/VE) composite by interleaving polyamide (PA) and polyethylene terephthalate (PET). PA cover showed better improvement than PET cover. The initial fracture toughness of the PA interleaved composite increased by 59% and the propagation interlayer fracture toughness increased by up to 90%. There are many studies in the literature of Polyamide-6.6 nanofibers with advantages such as high mechanical properties, high melting temperature, compatibility with uncured resin, processability, and higher fiber-forming ability. Also, it has features such as low heat deflection temperature and moisture absorption capacity. [29,32]. Sanatgar et al. (2012), examined polyamide 66 (SSP PA66) nanofiber with two different solution types and three different solution concentrations using the electrospinning method. The presence of chloroform at a concentration of 18 wt. % in the PA66/formic acid solution produced a reduction in crystallinity. The addition of chloroform at a concentration of 10 wt. % to the PA66/formic acid solution resulted in an increase in crystallinity from 28.5% to 43.1%. Beckermann and Pickering (2015), reported the effects of interspersed low-weight thermoplastic nanofiber covers on the Mod I, Mode II and interlayer fracture toughness of autoclaved unidirectional (UD) carbon/epoxy composite samples. Many different types of coatings were considered and 4.5 g/m2 PA66 cover " found to provide the best all-round fracture toughness performance with improvements of 156% for Mod I and 69%

for Mod II. Aljarrah and Abdelal (2019), studied the interlayer Mode I fracture toughness of Carbon fiber/epoxy laminates using a three-layer configuration. At the initial stage of crack propagation, up to 25% enhancement in interlayer fracture toughness was calculated for all configurations.

Electrospinning is one of the most effective, inexpensive and simple methods to produce continuous nanofibers, which can take full advantage of the properties of the solution components. In addition, electrospinning is a versatile method that includes polymer chemistry, electrical physics, fluid dynamics, basic physics, mechanical and textile engineering. In this method, it has been proven that it is possible to control fiber diameter and functionality by easily changing production and solution parameters such as voltage and solution composition. Therefore, nanofibers can be easily adapted to conventional composite fabrication techniques [36,37]. Van der Heijden et al. (2014), showed that the fracture toughness between composite laminates increased by adding poly-e-caprolactone nanofibers produced by electro-spinning method to the structure of the composites. Herwan et al. (2016), demonstrated that the load capacity of pin-bonded composite laminates could be increased by interspersing polyacrylonitrile (PAN) nanofibers on interlayer of carbon fabrics. The inclusion of micro or nanofillers in the resin liquid adversely affects the homogeneity and viscosity of the resin.Therefore, recently, there has been an increase in studies on the alternative production of fillers without being incorporated into the resin [29]. Bilge et al. (2014), obtained P(St-co-GMA) copolymer nanofibers using the electrospinning method. An 18 % increase was detected in the tensile strength of nanofiber reinforced composite structures. In addition, it has been shown that the maximum breaking stress is increased by 9 wt. % adding nanofiber interlayers to the regions exposed to high stress. In addition, nanofibers produced by electrospinning can be produced by adding filler materials such as CNT, graphene, nanodiamond. Studies are showing that structures can be strengthened by adding filler materials. Therefore, various methods have been developed, including chemical modification of nano carbons, namely improving the dispersion of CNTs, graphene and fullerenes [41].

# CHAPTER 3

# EXPERIMENTAL

## 3.1. Materials

In this study, (UD) unidirectional (carbon epoxy matrix based prepreg fabric, M91 / 34 / UD194 / IM7-12K) and (carbon epoxy matrix based prepreg fabric. M21 / HS / 40RC / T2 / AS4C / 285 / 6K) woven carbon fiber reinforced epoxy matrix based prepreg fabrics were used as primary reinforcement material. Unidirectional (UD) prepregs with a unit weight of 294 g / $m^2$ and woven prepregs with a unit weight of 475 g / $m^2$ were provided by Turkish Aerospace Industries Inc. Film adhesive (FM300K) was used as the adhesive tape.

Polyamide 66 (PA66) pellets have been used in their commercial forms to produce electrospun Polyamide 66 nonwoven fibers. Polyamide 66 pellets were dissolved in a mixture of formic acid and chloroform. The raw materials used for nanofiber production in this study are listed below;

- Polyamide 66 pellets (Sigma Aldrich- 429171)
- Formic acid (Sigma Aldrich- 27001)
- Chloroform (Sigma Aldrich- 24216)

The fiber morphology of Polyamide 66 nanofibers was investigated with a Scanning Electron Microscope (SEM). The average thickness of PA66 nanofibers was determined as 36.52nm. The melting point ($T_m$) and glass transition temperature ($T_g$) of PA66 nanofibers were determined using differential scanning calorimetry (DSC).

## 3.2. Preparation of PA 66 Nanofibers on Carbon Prepregs

The necessary literature research and trials were carried out for the electrospinning coating process, and the thermoplastic-based solution to be used for nanofiber production was determined as PA 66. The PA66 polymer solution was prepared following the procedure mentioned below. Before starting to prepare the solution, PA66 pellets were heated at 80 degrees for 24 hours to get rid of moisture. To

prepare PA 66 electrospun fibers, a 10 wt% solution of PA 66 was formed by dissolving 10 g of PA 66 pellets in 100 mL formic acid/chloroform (75:25 v / v) in atmospheric conditions. This concentration ratio was chosen based on the findings reported in previous works [29,33].

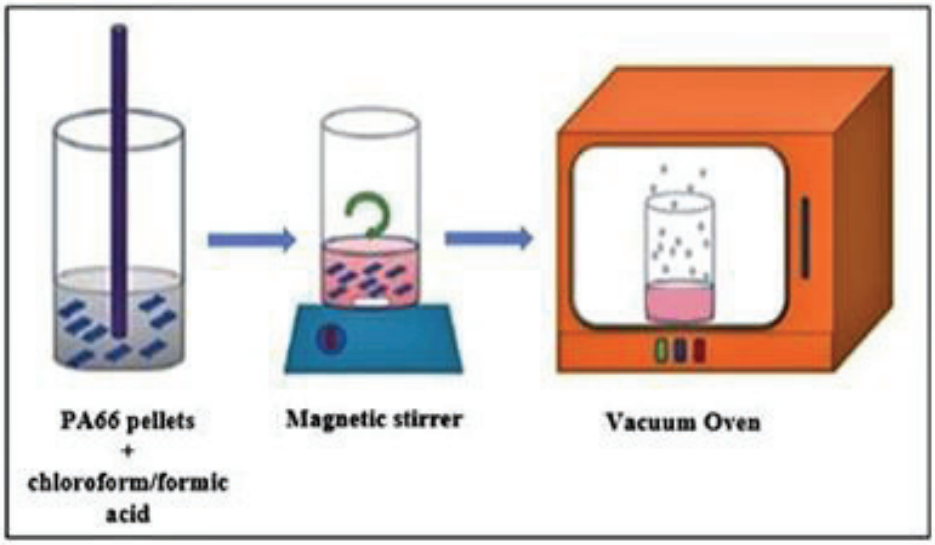


Figure 3. 1. Schematic representation of the solution preparation steps.

The solution with 10% PA 66 by weight was made by mixing 20 g of PA 66 pellets in 200 mL of formic acid and chloroform (150: 50 v / v) at room temperature on a magnetic stirrer for 12 hours. It was kept under a vacuum to remove bubbles before filling into syringes. The solution preparation process is summarized in Figure 3.1, schematically.

## 3.3. Coating of PA 66 Nanofibers on Carbon Prepreg

The dissolved PA66 polymer liquid was filled into two 50 mL syringes connected to the propellant pump. The flow rate of the liquid polymer solution was determined as 18 mL/hr (1.0 mL/hr for each nozzle). The voltage value to be applied during the coating was determined as 30 kV and the distance between the nozzle/collector was determined as 12 cm. The selected parameters were chosen based on our experience and data proven to be appropriate by Matulevicius et al. (2014). According to these parameters, homogeneous, one-dimensional and bead-free-homogeneous PA 66 nanofibers were

selected to produce. To get high efficiency from nanofibers, the INOVENSO PE300 device with homogeneity feature (z-axis movement) and the winding feature was used. Figure 3.2 shows the electrospinning setup used in this study.

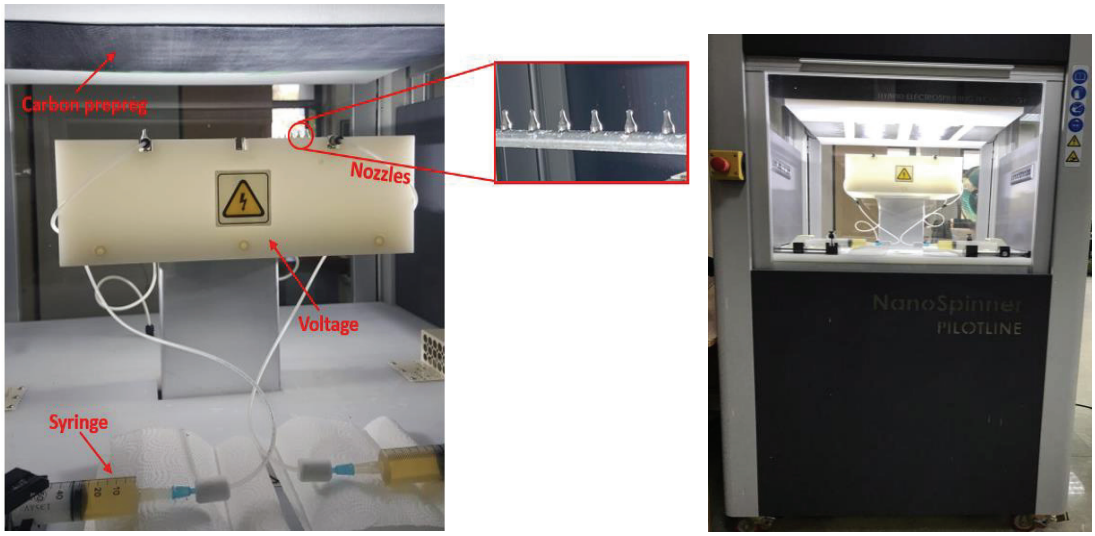


Figure 3. 2. Electrospinning devise in our laboratory.

The electrospinning time for PA66 nanofibers was chosen as 3 minutes, 7 minutes and 10 minutes. During the electrospinning process, the color of the carbon prepregs changed from black to white due to nanofiber deposition (Figure 3.3).

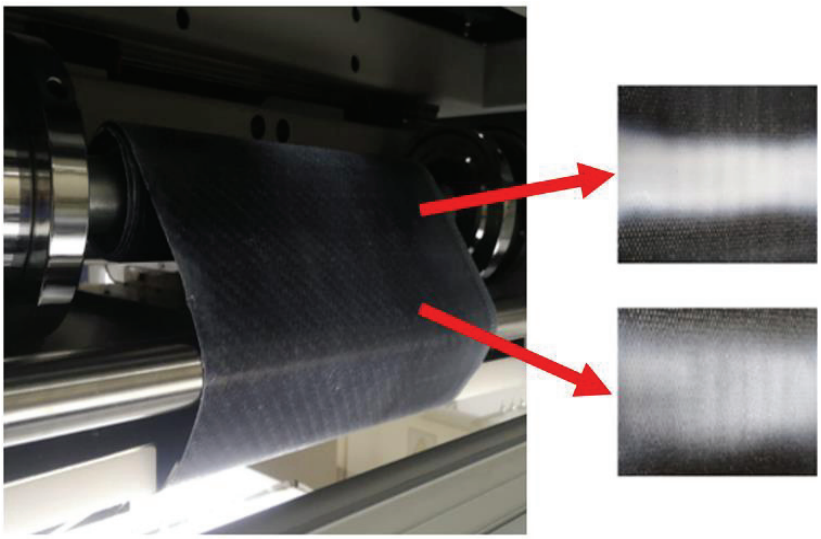

Figure 3. 3. Deposition of electrospun nanofibers on woven carbon prepreg.

Differential scanning calorimetry (DSC) device was used to analyze the thermal properties of the coated PA 66 nanofibers. The PA66 nanofiber sample from the coated prepreg was heated from room temperature to 350°C at a heating rate of 108 °C / min under nitrogen gas. The results of DSC analysis of PA 66 nanofibers are shown in Figure 3.4. The melting temperature (Tm) and Tg of PA66 nanofibers were decided as 261.41°C and 46.73°C, respectively.

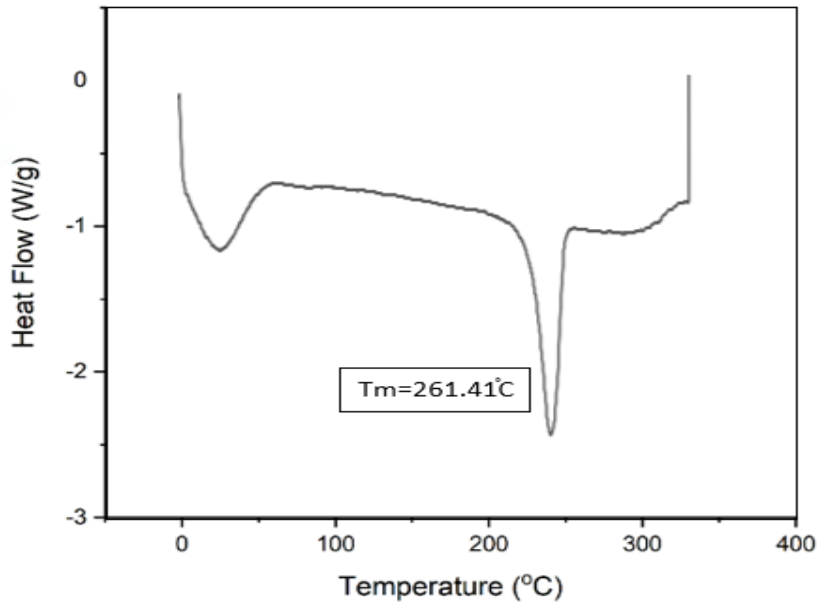


Figure 3. 4. DSC curve of the PA66 nanofibers.

Prepregs were coated with nanofibers for 3 minutes, 7 minutes and 10 minutes for Areal Weight Density (AWD) measurement. The PA66 nanofibers were stripped from the prepreg surface after coating and cut into small pieces of the same size. They were weighed with a 0.0001gr precision scale. The average PA66 nanofiber area weight density (AWD) for 3, 7 and 10 minutes deposition were determined to be approximately 0.525 g / $m^2$, 1.205 g / $m^2$ and 1.782 g / $m^2$, respectively.

Table 3. 1. Areal Weight Density (AWD) values of nanofiber coated prepregs

| **Spinning time** | **AWD (g/m2)** |
|---|---|
| 3 min | 0.525 |
| 7 min | 1.205 |
| 10 min | 1.782 |

As seen in Table 3.1, considering the AWD calculation, the effect of the coated nanofibers on weight gain is less than 2 %. For this reason, it has been determined that the effect of the coating on weight gain is negligible.

The fiber morphology of PA66 nanofibers was investigated with a scanning electron microscope (SEM). SEM images of nanofibers are shown in Figure 3.5. PA66 nanofiber diameters were determined as 36.52 nm on average. When the SEM images of the nanofibers produced with different solution trials were examined, it was decided to use a solution with a concentration of 10% PA66 by weight, where we could produce more homogeneous fiber.

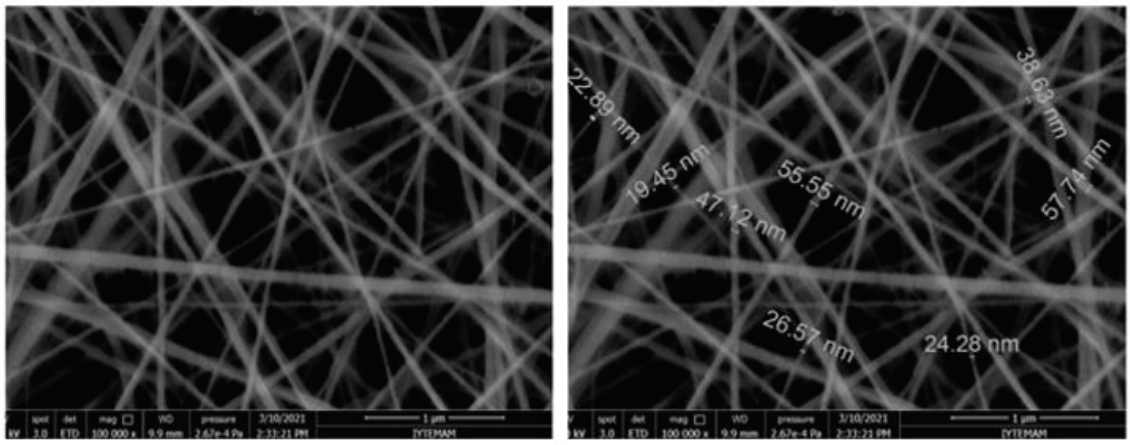


a)

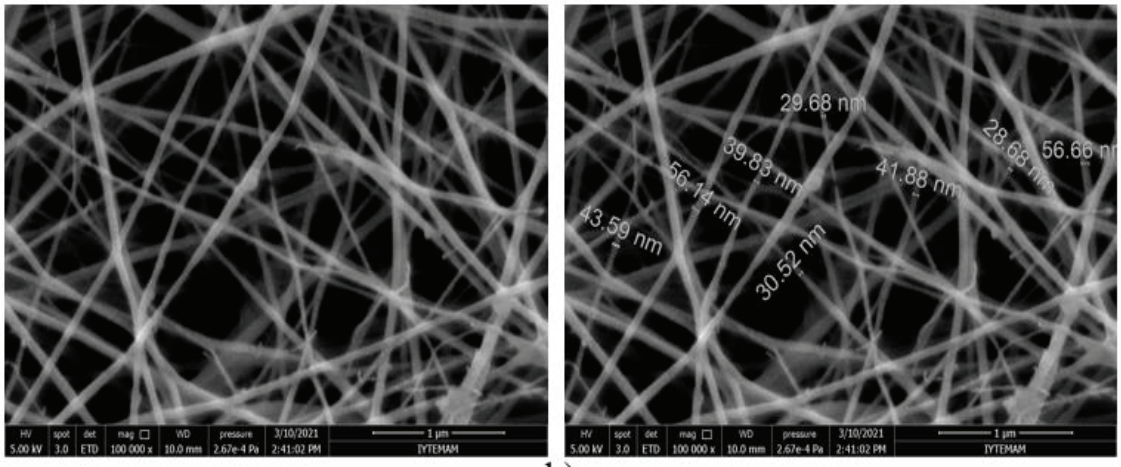


b)

**(cont. on next page)**

Figure 3. 5. a) 10% by weight PA66, b) 12% by weight PA66, c) 14% by weight PA66, d) 18% by weight PA66 nanofiber coating SEM images and nanofiber diameters

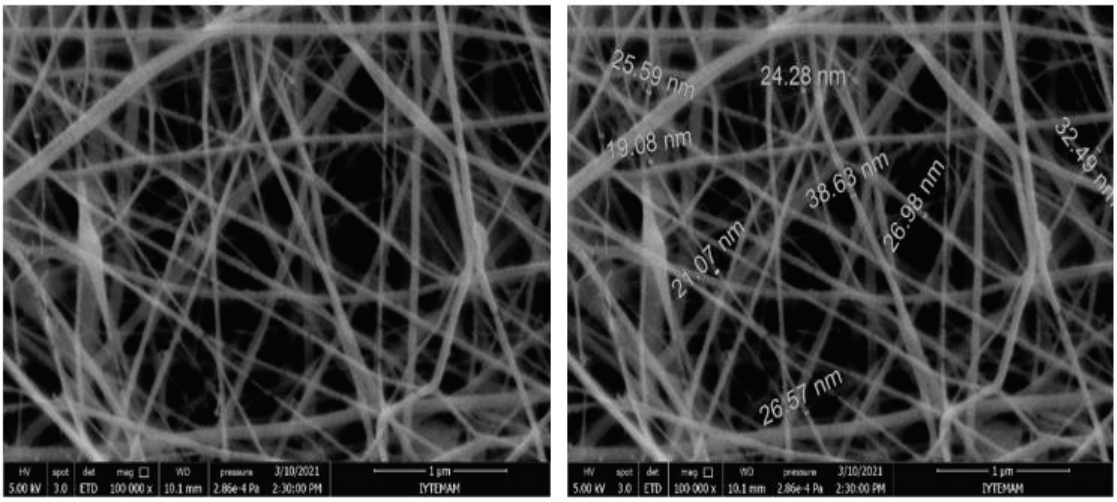


c)

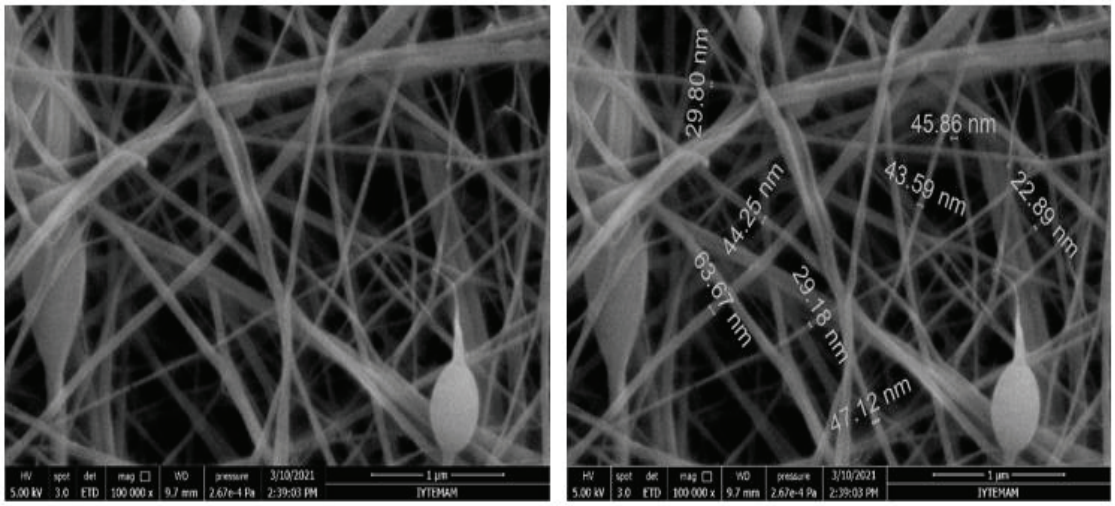


d)

Figure 3.5. (cont.)

## 3.4. Manufacturing of composite laminates

CFRF / PA66 plates with high-performance uniform fiber distribution were produced by the hot press method. Figure 3.6 shows the hot press setup used in this study. Prepregs were prepared based on the fabric properties specified in Table 3.2 were laminated under a hot press device for 2 hours at 180 ° C and 7 bar pressure.

Figure 3. 6. Plate production with the Hot Press method.

Table 3. 2. Adherend Material Types

| Prepreg Type | Material Name | Stacking Sequence | Plies |
|---|---|---|---|
| **UD** | M91 /34 /UD194 /IM7-12K | $[45/0/45/90/-45/0]_s$ | 12 |
| **Woven** | M21 /HS / 40RC /T2 /AS4C /285 /6K | $[45/0/45/0]_s$ | 8 |

Test samples were produced from composite laminates fabricated with UD and Woven prepregs with joint area coated PA66, by ASTM D5868 and ASTM D5528 standards as shown in Figure 3.7. FM300K film adhesive was used as the adhesive material to produce lap shear test samples containing nanofibers coated on the prepregs. FM300K has been used in two different layers (2 layers (0.4mm) and 3 layers (0.6mm)). Two different types of laminate made of composite prepreg were used as adherent material: UD and Woven (Table 3.3). Prepregs were left to cure for 150 minutes under 3 bar pressure in a hot press device previously adjusted to 180 ° C. The produced composites were cut by the standards with a wet saw cutting device. The edges of the cut samples were gently sanded with sandpaper. The test specimens cut in the wet cutting device were left to dry for 1 hour at 50 °C. The average thickness of the composite samples was measured as 2.47 mm.

Table 3. 3. Test sample production conditions.

| **Laminate Type** | **Adhesive Type** | **Bondline Thickness (mm)** | **Test Temperature** |
|---|---|---|---|
| **UD + Woven** | Film | 0.60 (3plies) | RTD |
| **UD + Woven** | Film | 0.40 (2plies) | RTD |

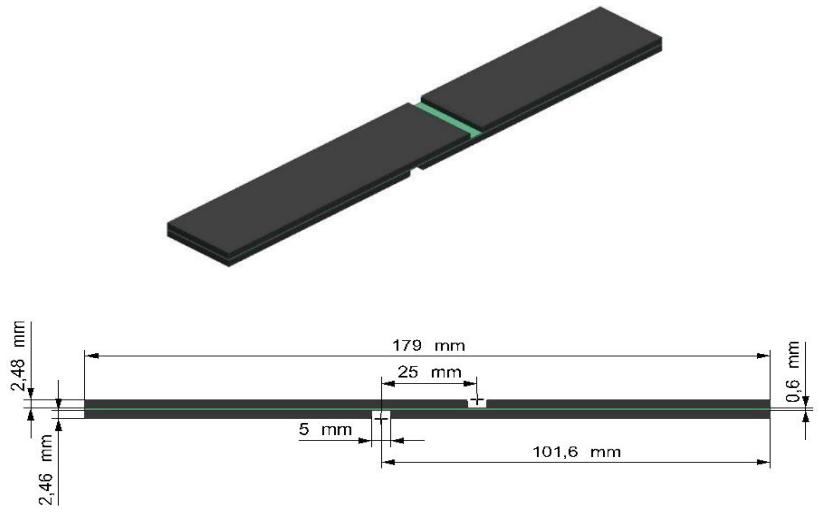


Figure 3. 7. Fabric alignment of UD and Woven plates and production of lap shear test coupons.

For the Mod-I fracture toughness tests, a nanofiber cover was placed between the ninth and tenth layers of 18-layer prepreg fabrics. For other in-plane mechanical tests, nanofibers were placed in the joint area. A Kapton film (50 μm thick) was interposed to create an initial crack along the junction between the two plates of the DCB samples. The dimensions of the samples prepared for DCB testing are shown in Figure 3.8.

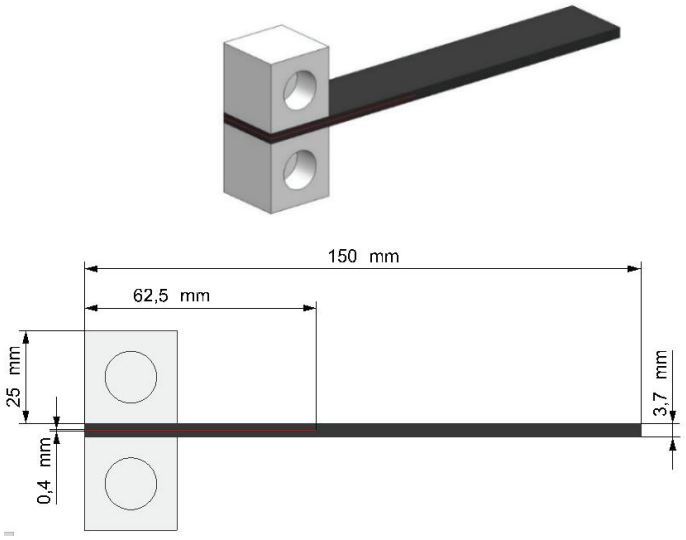


Figure 3. 8. DCB samples shown schematically

## 3.5. Mechanical characterization of composite specimens

Tensile, three-point bending, compression, single-lap shear, mod-I fracture toughness and charpy impact tests were performed to define the effects of PA66 covers on the mechanical properties of CF/EP prepreg composites. All mechanical tests are carried out in atmospheric conditions according to compliance specified in ASTM and ISO standards.

### 3.5.1. Single Lap Shear Tests

All mechanical tests have been done according to the relevant ASTM 5868-01 standards. The lap joint tester is shown in Figure 3.9. An MTS Landmark™

Servohydraulic Test System is used. The load applied during the test was applied at a speed of 13 mm/min according to the ASTM D5868-01 standard.


Figure 3. 9. Test set-up for the single-lap joint.

Single lap shear test used for determining the bonding properties of adhesive for joining UD and Woven and determining the shear strength of the joints. Prepared test coupons are shown in Figure 3.10.

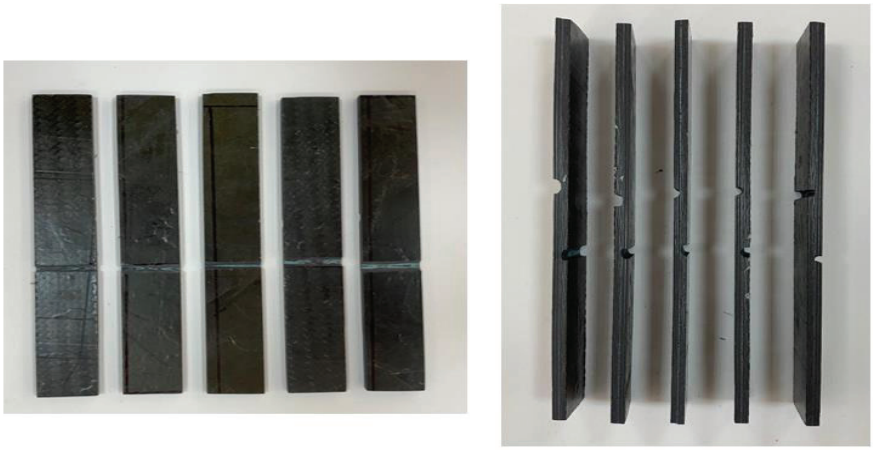

Figure 3. 10. Test specimens joined by the secondary bonding method.

After the single lap shear strength test, to determine the types of failure (adhesive, cohesive or mixed adhesive-cohesive) the adhesion surfaces of the specimens which were exposed to the lap shear test were examined.

### 3.5.2. Tensile Tests

The tensile strength, strain, and modulus of elasticity of the specimens were calculated by the tensile test. Test samples were prepared according to the ASTM D 3039M-93 test standard. 5 specimens with a width of 25 mm and a length of 250 mm were cut from a 300 x 300 $mm^2$ plate. Samples were tested at room temperature. A tensile test at a crosshead speed of 2 mm/min was performed with the MTS Landmark™ Servohydraulic System with a dynamic 100 kN / 22 kip and a static 120 kN / 27 kip capacity load cell. Displacement values were calculated using an extensometer. Figure 3.11 shows a visual from the moment of the tensile test.


Figure 3. 11. Tensile test specimen under tension

### 3.5.3. Three-Point Bending Tests

Three-point bending test specimens were prepared according to the ASTM D790 test standard. The bending properties of the samples were obtained from the three-point bending test. The test was performed using the MTS Landmark™ Servohydraulic Test System and the crosshead speed of the test machine was set at 2 mm/min. The test specimens were cut 10 mm wide and 145 mm long. The lengths of the samples were associated with the aperture ratio specified in the standard and the support span ratio was chosen as 32 according to the specimen type. Figure 3.12 shows a picture of the three-point bending test apparatus.

Figure 3. 12. Test Specimen Under Flexural Loading

Cross Head movement speed is calculated according to Eq 1[43]:

$$R = ZL^2/6d \quad (1)$$

Z shall be equal to 0.01.

Flexural Stress can be calculated by selecting any point on the load-deflection curve with Equation 2 below [43]:

$$\sigma_f = 3PL/2bd^2 \quad (2)$$

Flexural Strain can be calculated for any deflection using Equation 3[43]:

$$\varepsilon_f = 6Dd/L^2 \quad (3)$$

The modulus of elasticity is calculated using Equation 4 shown below and drawing a tangent from the origin of the load-deflection curve to the straight-line portion on the curve [43].

$$E_B = L^3m/4bd^3 \quad (4)$$

### 3.5.4. Compression Tests

Compression test specimens were prepared by the ASTM D695-02 standard. Samples were cut to 12.7 mm in width and 140 mm in length. An anti-buckling apparatus was used during the test to calculate the compressive modulus and strength of the prepared samples (Figure 3.13). Samples were loaded until fracture at a constant crosshead speed of 1.3 mm/min.

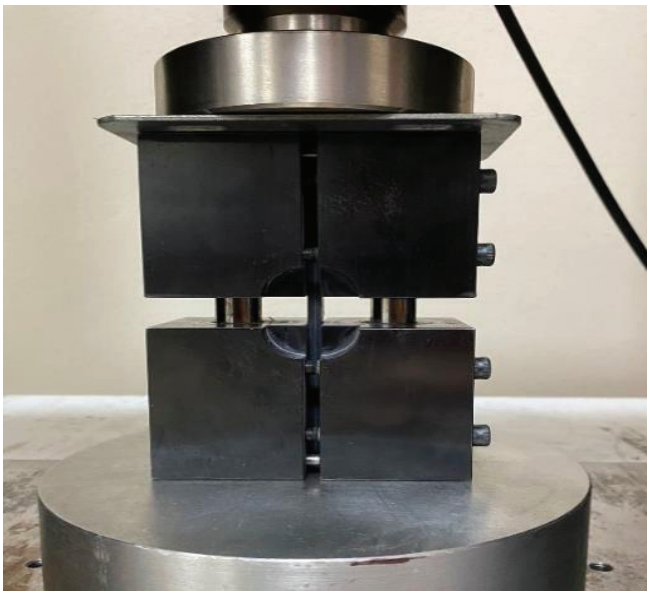

Figure 3. 13. Test Specimen Under Compression Loading

### 3.5.5. Charpy-Impact Tests

The CEAST® Resil Impactor, which has a maximum energy of 15 J - 25 J and a tangential speed of 3.46 m/s, was used for the Charpy impact tests. The samples were produced by cutting 10 x 80 mm rectangles and notching 2 mm following the ISO-179 standard. Charpy impact strength is calculated by dividing the energy by the notched area. At least ten samples were tested for each group to obtain consistent mean and standard deviation values.


Figure 3. 14. Test set-up for the single-lap joint.

### 3.5.6. Mode-I fracture toughness tests

Mod-I laminar fracture toughness of composite samples was analyzed by double cantilever beam (DCB) test using Shimadzu AGS-X, Kyoto, Japan, test device with 5 kN load cell. Samples were initially loaded at a rate of 1 mm/min and the fracture was allowed to travel a short distance (3-5 mm). Then, the load was applied to propagate the crack formed in the sample by approximately 70 mm. To calculate the Mod I laminar fracture toughness, the laminar fracture toughness ($G_{ıc}$) values of the load, displacement and crack lengths of the samples were calculated during the test. The $G_{IC}$ value of the delamination was calculated by visually observing the initial $G_{IC}$ ($G_{IC,ini}$) value from the criterion drawn on the cracked surface of the sample. The $G_{IC}$ spread ($G_{IC,prop}$) value was

determined by averaging the crack propagation and $G_{IC}$ values. Figure 25 shows an example of a DCB under Mode-I loading. $G_I$, $G_{IC,ini}$ and $G_{IC,prop}$ values were determined by the Modified Beam Theory data reduction method. [31,44].

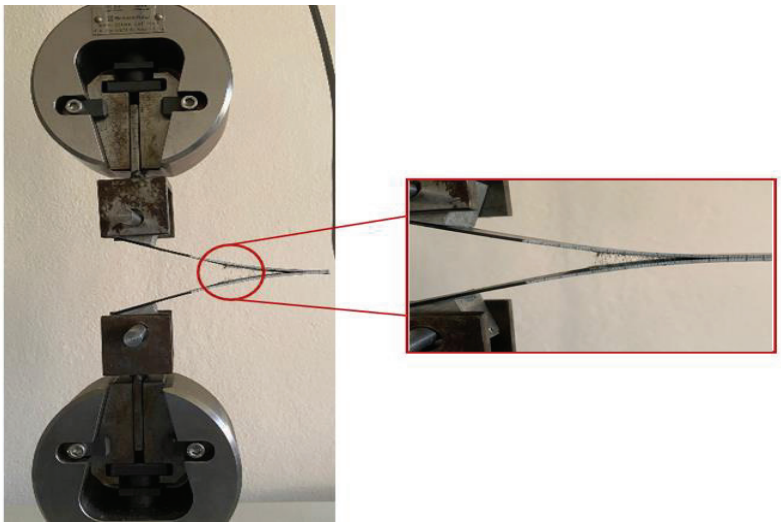

Figure 3. 15. Test set-up for the single-lap joint.

Double cantilever beam (DCB) experiments were completed to calculate the Mod-I interlayer fracture toughness of the composite samples. The sample preparation scheme for the DCB test is shown in Figure 3.15.

DCB samples were prepared by cutting 150 mm (L) long and 25 mm (b) wide. To transfer the opening force to be applied to the DCB specimens during the test, aluminum cubes were attached to the specimen surfaces. Before testing, one edge of the samples was painted white and measured as a ruler at 1 mm intervals to observe crack propagation. The force was applied until the first separation of the test sample was completed, then it was zeroed. After the samples were subjected to force again, the displacement and fracture progression length values were recorded. Each sample was first loaded at a crosshead speed of 1 mm/min and the fracture was allowed to advance 2-6 mm before unloading from the sample. Then, the first crack was exposed to load until it progressed 50-60 mm. During the tests, the load of the sample, crack opening displacement and crack length were noted for energy release rate ($G_I$) analysis. The $G_I$ was determined according to the following data reduction method in the standard [45].

$$G_I = \frac{3P\delta}{2b(\alpha + |\Delta|)} \quad (5)$$

The $G_I$ in the equation is the Mode I interlayer fracture toughness. *P, b, a,* and $\delta$ is called *a* load, specimen width, delamination length and load point displacement, respectively. Δ is a value calculated experimentally by constructing a least-squares plot of the root of feet ($C^{1/3}$) as an equation of crack length. F and N are the error parameters used to calculate the displacement and hardening of the specimens. F considers the shortening of the moment arm and bending of the end blocks. N considers the hardening of the sample by the blocks. These correction factor equations are given below [45];

$$F = 1-(\frac{3}{10})(\frac{\delta}{\alpha})^2 - (\frac{3}{2})(\frac{\delta t}{\alpha^2}) \quad (6)$$

$$N = 1-(\frac{L'}{\alpha})^3 -(\frac{9}{8})\left[1 - \left(\frac{L'}{\alpha}\right)^2\right]\left(\frac{\delta t}{\alpha^2}\right) - \frac{9}{35}(\frac{\delta}{\alpha})^2 \quad (7)$$

The t and L' values in the samples are displayed in Figure 3.16. The initial $G_{IC}$ ($G_{IC,ini}$) data was calculated as $G_{IC}$ data in which crack propagation was observed based on measurements plotted at one edge of the sample. $G_{IC}$ spread ($G_{IC,prop}$) data was analyzed by averaging the $G_{IC}$ values during delamination progression. Figure 3.1m shows the behavior of a composite test specimen during Mode-I loading.

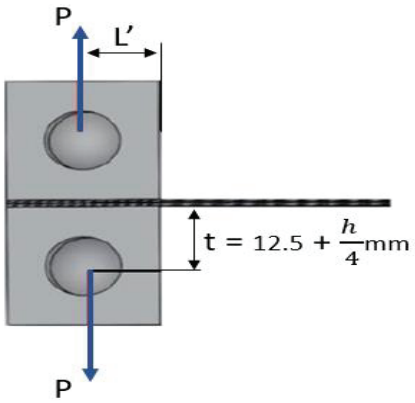


Figure 3. 16. Dimensional relationship between the DCB test specimen and the aluminum blocks adhered to it to transfer the opening forces

# CHAPTER 4

# RESULTS AND DISCUSSION

## 4.1. Nanofiber Morphology

SEM images of PA66 nanofibers produced by electrospinning are shown in Figure 4.1. Bead-free, continuous and smooth, homogeneous nanofibers were obtained with optimized spinning parameters. Eight different nanofibers were measured to calculate the average diameter of the nanofibers. The mean nanofiber diameter was determined as 36.52 ± 12 nm. In addition, it has been proven in the literature that the addition of nanofibers between the layers of composites has a significant effect on fracture toughness [29].

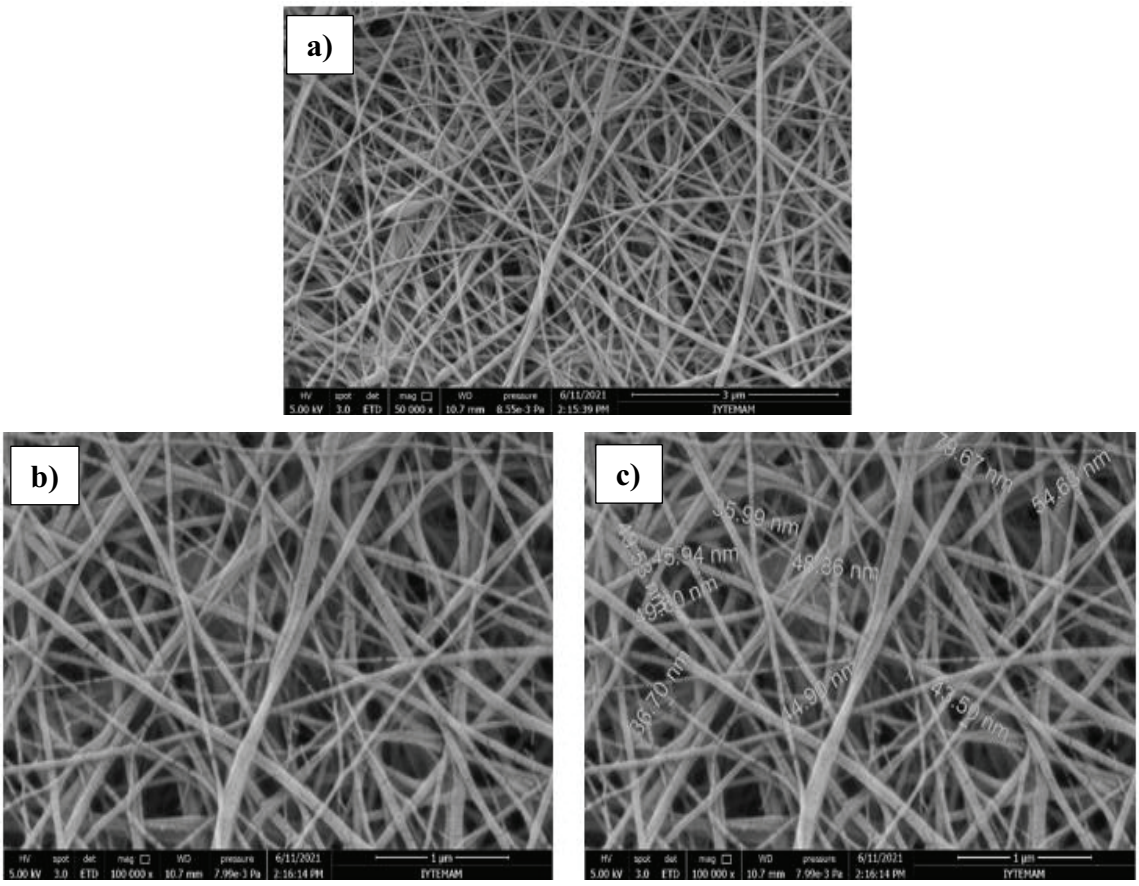


Figure 4. 1. SEM images of 10 wt% PA 66 nanofibers at (a) 50,000X, (b)100,000X and (c) 100,000X magnification.

When the SEM images in Figure 4.2 are examined, the 10 weight percent solution ratio we have chosen as the coating parameter and the 10 minute coating time provide more homogeneous fiber production compared to other parameters.

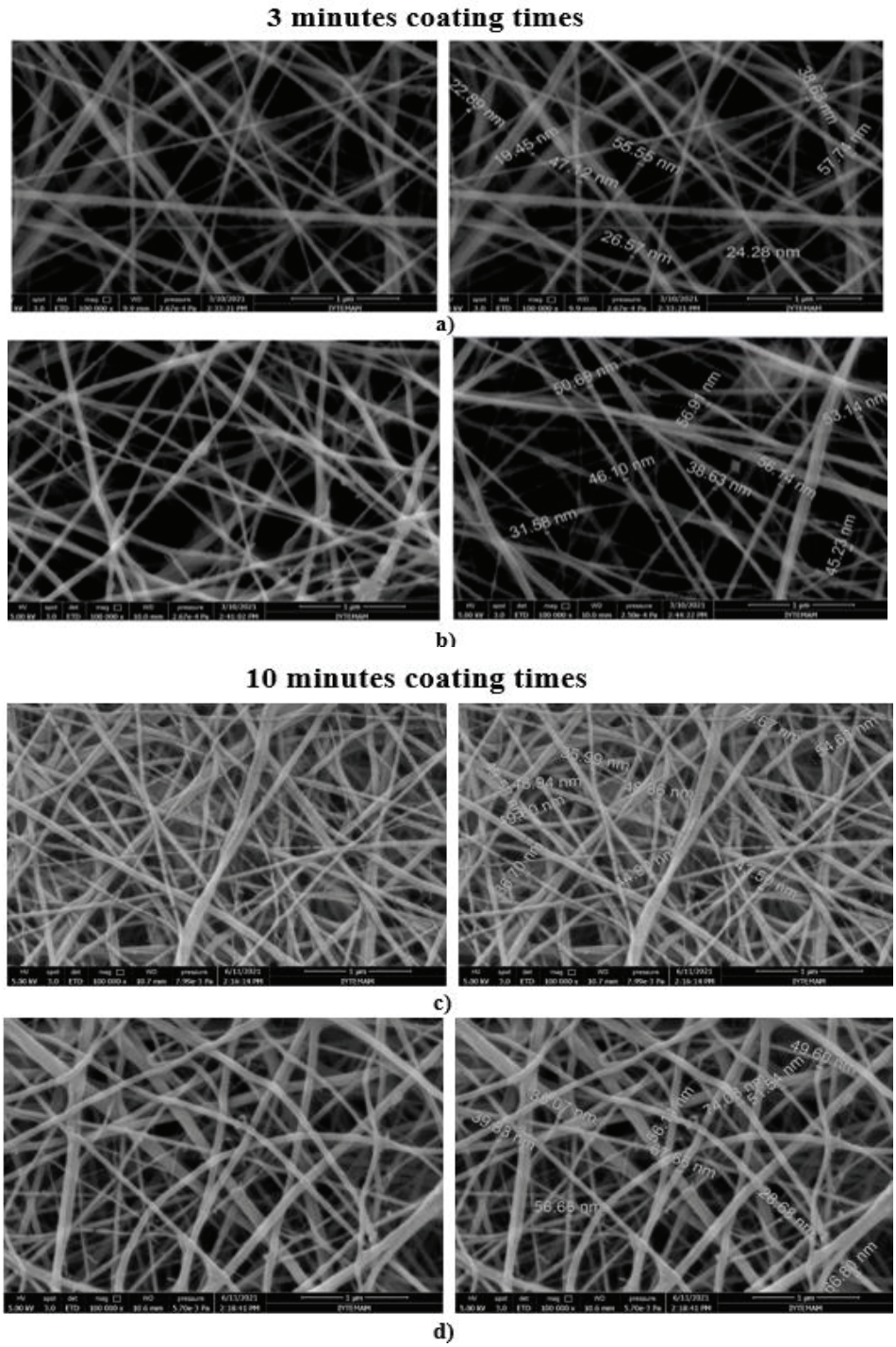


Figure 4. 2. SEM images of nanofibers at a) 10% PA66-3 min., b) 18% PA66-3 min., c) 10% PA66 -10 min. and d) 18% PA66-10 min. two different solution ratios and coating times.

## 4.2. Surface Roughness Characterization

Surface roughness and coating surface properties (Ra, Rz, Rq, Rt) of reference and PA66 nanofibers were measured using a profilometer surface roughness tester. The set-up parameters of the device are respectively; size=4500x100 and sampling are determined as 1.11un. For both surfaces, the average surface roughness values were determined by measurements taken from five random surface points. As a result of these measurements, it was determined how much the surface roughness increased by adding PA66 nanofibers to the surface.

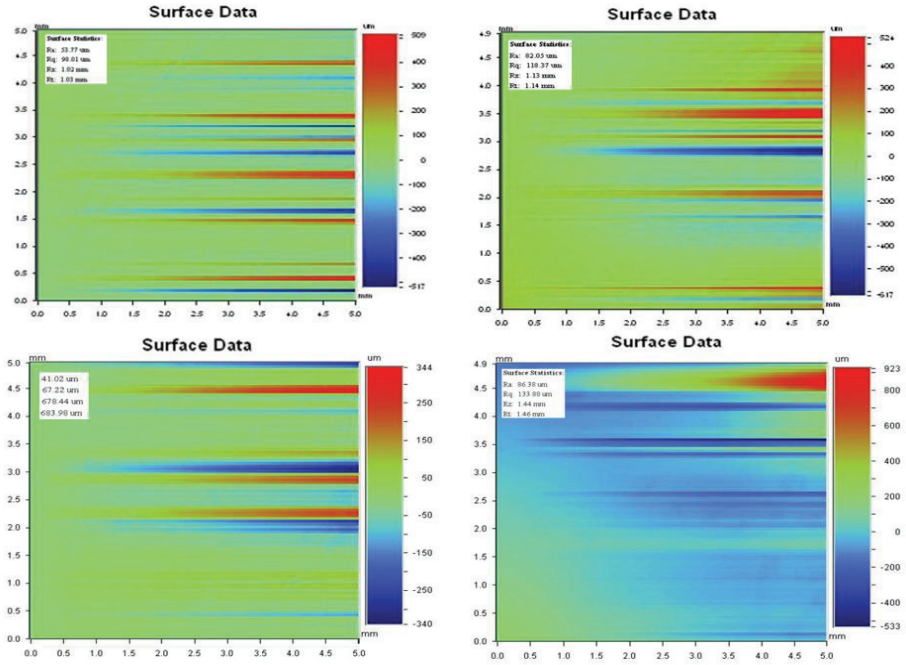


Figure 4. 3. Surface roughness and coating surface properties (Ra, Rz, Rq, Rt) of reference and PA66 nanofibers

## 4.3. Mechanical Properties of CFP/PA66 Composite Plates

In this section, the mechanical, thermal and microstructural properties of UD and woven prepreg based laminates, which are first coated with PA66 and then bonded with the secondary bonding method, are presented.

### 4.3.1. Single Lap Shear Tests

The shear properties of composite specimens cured at 180°C and 7 bar pressure and coated with PA66 in the joint area were investigated. Lap shear tests were performed by ASTM D5868. To evaluate the adhesion strength of UD and Woven CF/EP prepreg plates bonded with FM300K film adhesive, samples were prepared with two different amounts of adhesive. These adhesive plies (2-3 plies) were chosen to keep the thickness increase to a minimum. The nanofibers produced with 3 different (10-12% and 14% wt) solution ratios on the adhesion surfaces of the prepregs to be modified were interspersed with a 10-minute coating time selected according to the SEM results. Optimum parameters of the study were determined by choosing the parameter that provides the best increase among these 3 different solutions and 2 different adhesive layers. When the test results in Figure 4.4 are examined, the highest increase in bond strength was observed in the samples containing 10% by weight PA66.

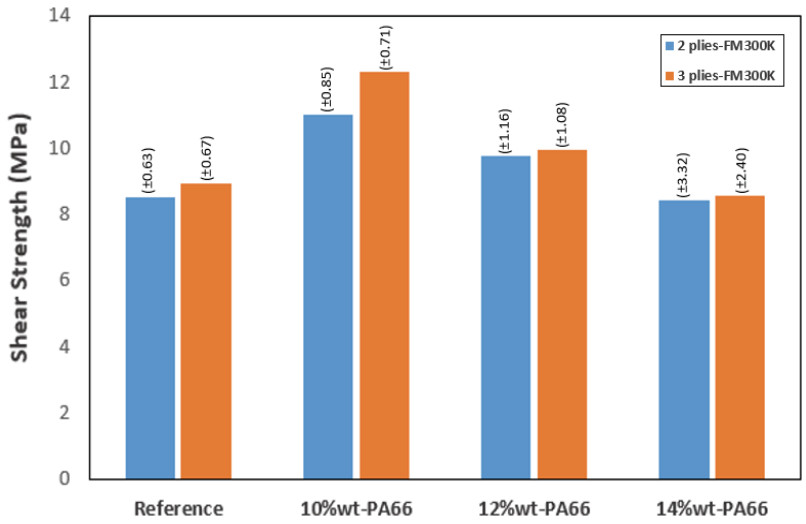


Figure 4. 4. The lap shear values of test specimens.

Shear load-extension diagrams of samples produced using 10% wt-PA66 nanofiber coated, 2-layer and 3-layer adhesive are shown in Figure 4.5. These results were calculated based on the force-displacement curve and the cross-sectional area of the test specimens.

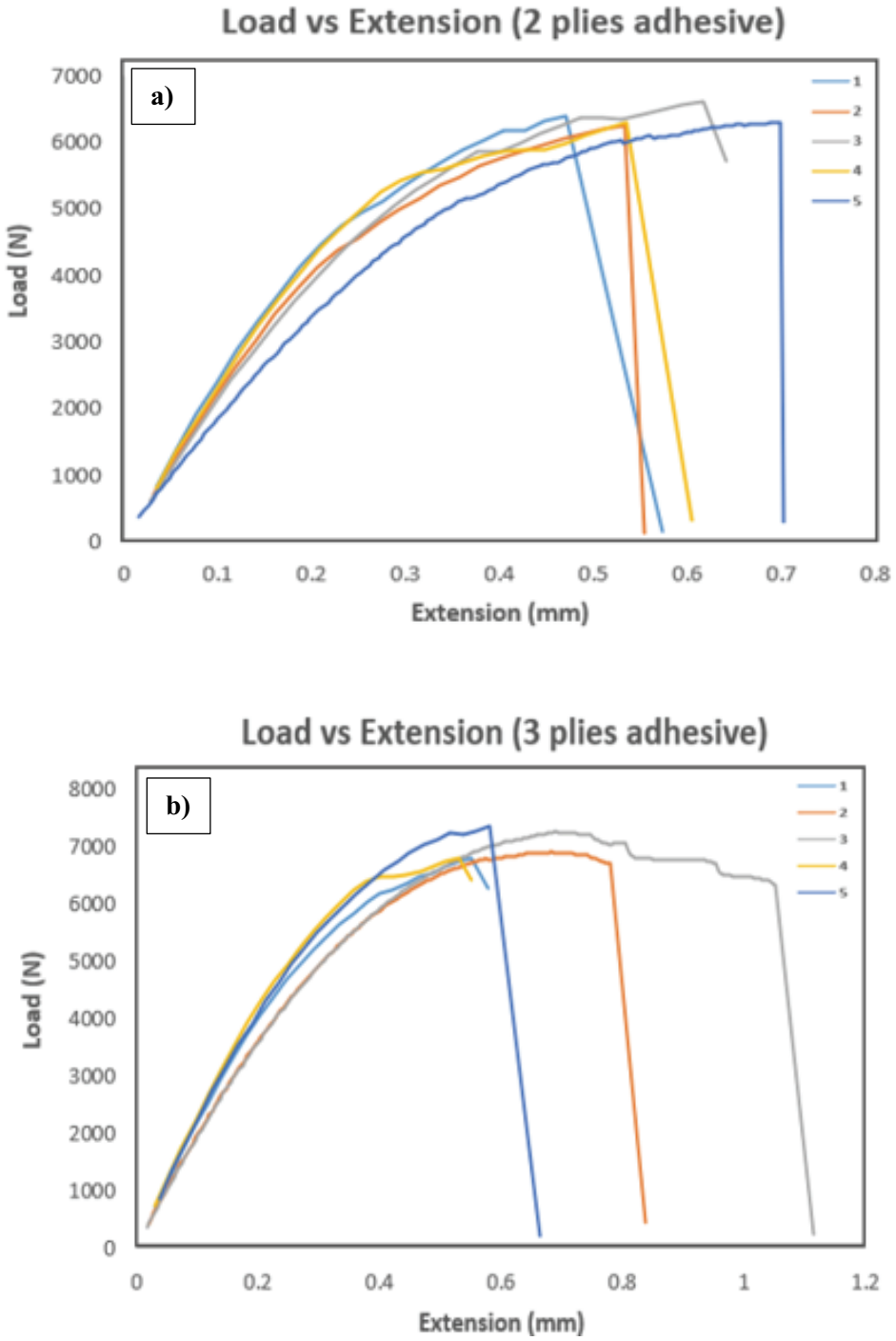


Figure 4. 5. Load vs. extension curves of a) 10%wt-PA66-2pliesFM300K and b)10%wt-PA66-3pliesFM300K specimens according to single lap shear test.

Table 4. 1. Test sample production conditions.

| Test Sample | Nanofiber Material | Shear Strength (MPa) | Standard Dev. (±) | Improvement or Reduction (%) |
|---|---|---|---|---|
| **Reference 2plies** | - | 8.50 | 0.63 | - |
| **Reference 3plies** | - | 8.91 | 0.67 | - |
| **2 plies FM300K** | 10%wt PA66 (10 min) | 10.99 | 0.85 | **+29.29** |
| **3 plies FM300K** | 10%wt PA66 (10 min) | 12.32 | 0.71 | **+38.27** |

Table 4.1 summarizes the lap shear test results of composite specimens with 10%wt - PA66 added to the reference and attachment region. Both the reference samples and the PA66 nanofiber reinforced samples show a linear elastic behavior up to fracture. In Table 4.1, the shear strengths of the reference composites produced with 2-layer and 3-layer adhesive are 8.50 MPa and 8.91 MPa, respectively. The shear strength of the PA66 nanofiber added samples, which were bonded with 3 layers of film adhesive, showed an improvement of 38.27% compared to the reference sample. Compared to 2 layers of film adhesive, samples with 3 layers of film adhesive showed higher performance.

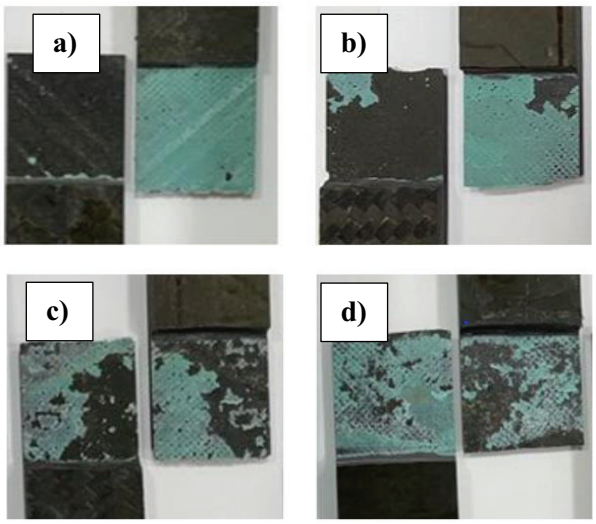


Figure 4. 6. The fracture surface of a) 2plies/FM300K reference samples, b) 3plies/FM300K reference samples, c)10wt% PA66-10min /2 plies FM300K, d) 10wt% PA66-10min /3 plies FM300K specimens after single lap shear test

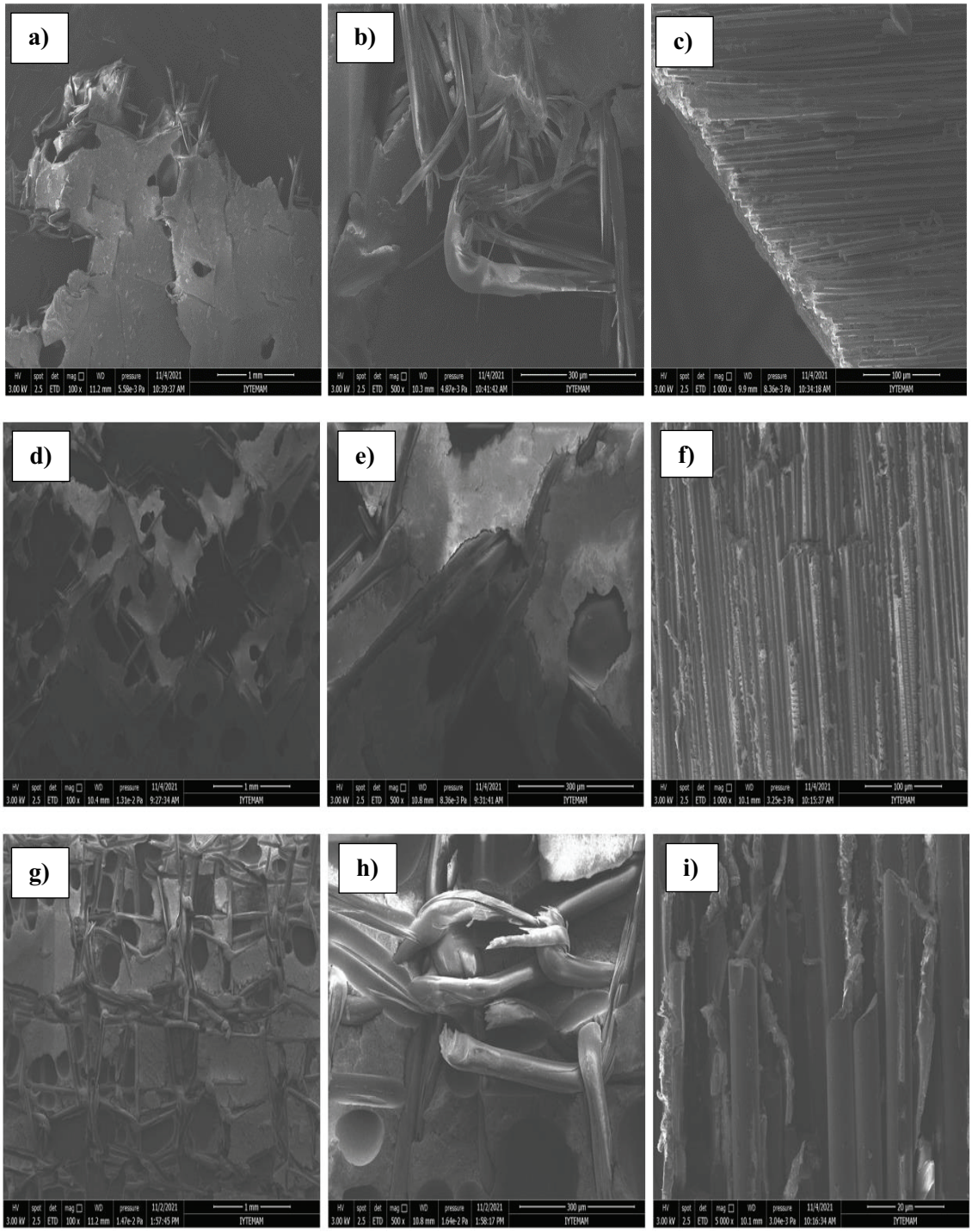


Figure 4. 7. Shows the junction region SEM images of the a-b-c) reference, d-e-f) 2-plies adhesive and g-h-i) 3-plies adhesive PA66 spliced lap-shear specimens.

Figure 4.6 and Figure 4.7 show the joint area and SEM images of the reference and PA66 modified composites after the lap shear test. When the fracture surfaces of the joint area were examined, it was observed that the PA66 modified samples adhered better to the adhesive than the reference samples. When the samples combined with 2 layers and 3 layers of adhesive were compared with each other, it was determined that the samples combined with 3 layers of film adhesive showed better adhesion performance than the samples combined with 2 layers of film adhesive. When the test results were examined, it was proved that the coating of PA66 nanofibers on prepregs showed a striking increase in bond strength. The resulting structure is a good method to reduce joint area fragility.

### 4.3.2. Tensile Tests

The tensile properties of the composite samples, which were cured and joined at 180°C and 7 bar pressure, in which the joint area was coated with PA66, were investigated. Tensile tests were carried out according to ASTM D3039. The tensile behavior of the reference samples is shown in Figure 4.8. The tensile strength and elastic modulus of the reference samples in Table 4.2 were calculated as 628.93 MPa and 53.17 GPa, respectively.

Table 4. 2. Tensile properties of reference samples.

| Sample Name | Tensile Strength (MPa) | Max. Force (N) | Elastic Modulus (GPa) | Strain at Break (%) |
|---|---|---|---|---|
| **R1** | 645.84 | 81.49 | 52.67 | 1.29 |
| **R2** | 615.58 | 72.19 | 46.49 | 1.35 |
| **R3** | 631.31 | 80.92 | 53.48 | 1.25 |
| **R4** | 639.42 | 81.27 | 57.81 | 1.04 |
| **R5** | 612.52 | 76.80 | 55.42 | 1.00 |
| **Avg.** | **628.93** | **78.53** | **53.17** | **1.18** |
| **St. Dev. (±)** | **13.03** | **3.61** | **3.78** | **0.13** |

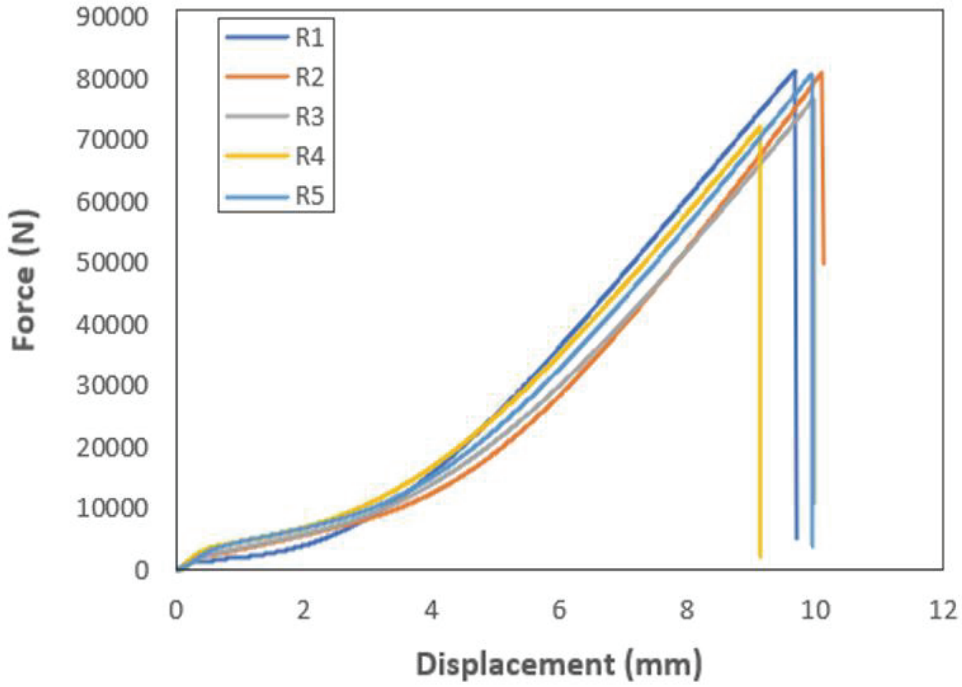


Figure 4. 8. Force vs displacement curve of reference samples under tensile loading.

Table 4. 3. Tensile properties of PA66 added samples.

| Sample Name | Tensile Strength (MPa) | Max. Force (kN) | Elastic Modulus (GPa) | Strain at Break (%) |
|---|---|---|---|---|
| **1** | 675.99 | 87.31 | 55.89 | 0.99 |
| **2** | 707.83 | 88.65 | 50.71 | 1.45 |
| **3** | 678.53 | 85.25 | 65.38 | 0.95 |
| **4** | 705.05 | 91.93 | 51.59 | 1.23 |
| **5** | 697.18 | 87.75 | 49.23 | 1.22 |
| **Avg.** | **692.91** | **88.17** | **54.56** | **1.16** |
| **St. Dev. (±)** | **13.27** | **2.18** | **5.84** | **0.18** |

It is shown in Table 4.3 that the addition of PA66 nanofibers to the junctional region increased the elastic modulus of the composites from 53.17 GPa to 54.56 GPa. The tensile behavior of the samples containing PA66 is given in Figure 4.9. These results were calculated based on the force-displacement curve and the cross-sectional area of the test specimens.

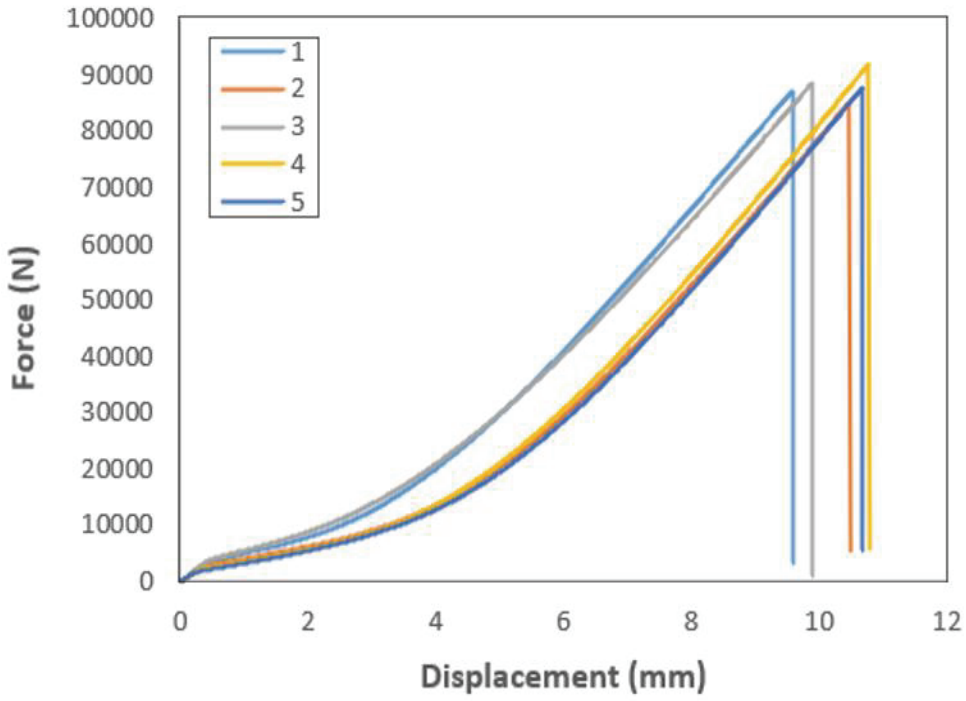


Figure 4. 9. Force vs displacement curve of PA66 added samples under tensile loading.

The increase in tensile strength and elastic modulus was 10.17% and 2.61%, respectively. These results, stated in the literature, "The void occurring in PA66 interspersed composite materials causes a decrease in the tensile properties of the samples." refuted his opinion. This is because the amount of PA66 nanofibers added was not large and these nanofibers changed the thickness of the sample negligibly. One of the most important reasons for these increases is the improvement of the matrix cracking resistance of the samples with PA66 nanofibers added to the junction area. SEM images of the matrices of deformed reference and PA66 added composites are shown in Figure 4.10. The presence of PA66 nanofibers in the matrix enables the matrix to withstand higher loads in the tensile direction, increasing the tensile strength values of the nanofiber-coated specimens in the joint zone. The nanofibers added to the joint area act as veils and allow the adhesive to adhere better to the fibers. Compared to the reference samples, it was observed that the nanofiber-added composites showed better mechanical bonding performance. These results are supported by the data in the tensile test results.

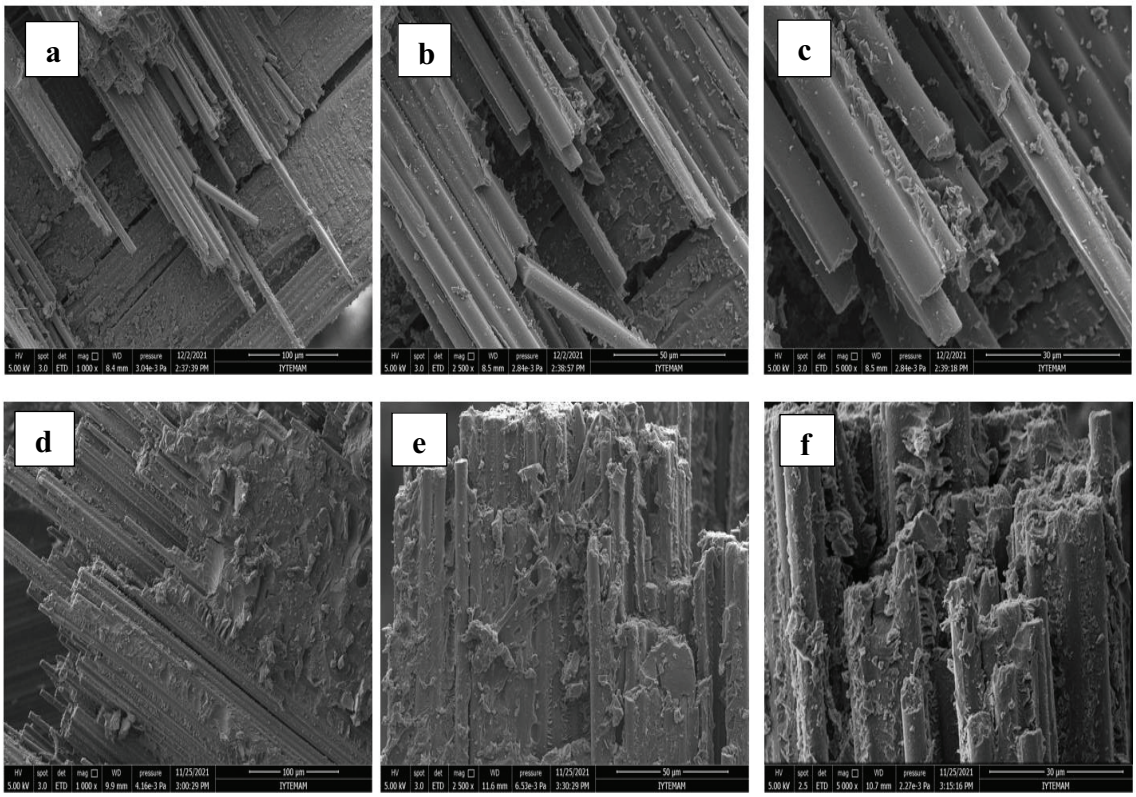


Figure 4. 10. a-b-c)Reference and d-e-f)SEM images of the deformed region of the samples with PA66 added

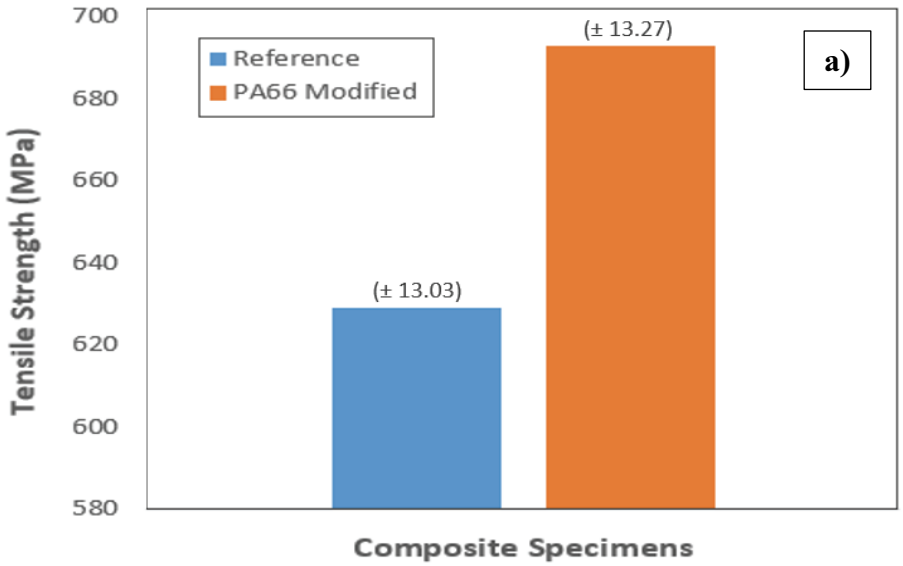


**(cont. on next page)**

Figure 4. 11. a) Tensile strength and b) Elastic modulus values of the Reference and PA66 added samples

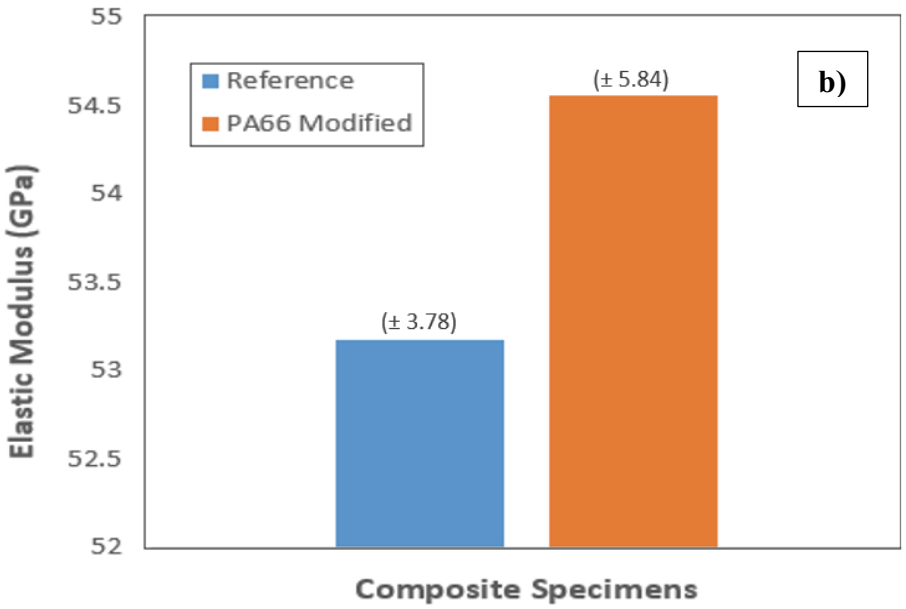


Figure 4. 11. (cont.)

Figure 4.11 and Table 4.4 summarize the tensile test results of the reference and nanofiber coated samples. The addition of PA66 to the samples did not significantly change the AWD value and thickness of the samples. The tensile strengths of the PA66 added samples were increased by approximately 10.17% compared to the reference samples. This increase was interpreted to be related to the decrease in stress concentrations of the PA66 nanofibers samples. Studies of Bilge et al. and Beylergil et al. in the literature support this interpretation.

Table 4. 4. Summary of tensile test results.

| Sample Name | Tensile Strength (MPa) | Max. Force (kN) | Elastic Modulus (GPa) | Strain at Break (%) |
|---|---|---|---|---|
| **Reference Avg.** | 628.93 | 78.53 | 53.17 | 1.18 |
| **St. Dev. (±)** | **13.03** | **3.61** | **3.78** | **0.13** |
| **PA66 Modified Avg.** | 692.91 | 88.17 | 54.56 | 1.16 |
| **St. Dev. (±)** | **13.27** | **2.18** | **5.84** | **0.18** |

### 4.3.3. Three-Point Bending Tests

The bending properties of the composite specimens whose junction area was coated with PA66 were investigated. Bending tests were carried out according to ASTM D790. Figure 4.12 and Figure 4.13 show the force-displacement curves of the reference and PA66 interspersed specimens under bending loading, respectively.

Table 4. 5. Flexural properties of reference samples.

| Sample Name | Flexural Stress (MPa) | Max. Force (N) | Flexural Strain (%) | Max. Stroke (mm) |
|---|---|---|---|---|
| **R1** | 445.05 | 430.00 | 0.91 | 6.76 |
| **R2** | 386.39 | 385.00 | 0.70 | 5.33 |
| **R3** | 456.51 | 427.66 | 0.87 | 6.32 |
| **R4** | 422.85 | 430.63 | 0.69 | 5.27 |
| **R5** | 470.49 | 471.56 | 0.75 | 5.74 |
| **Avg.** | **436.25** | **428.97** | **0.78** | **5.88** |
| **St. Dev. (±)** | **29.41** | **27.39** | **0.08** | **0.57** |

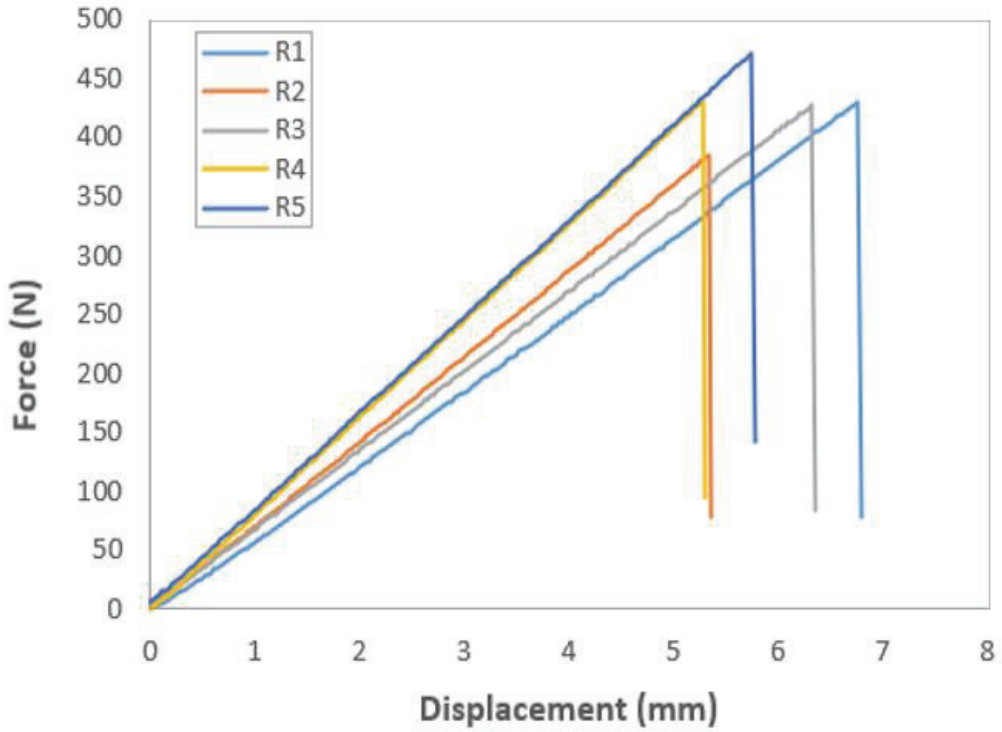


Figure 4. 12. Force vs displacement curve of reference samples under flexural loading.

Table 4. 6. Flexural properties of P66 added samples.

| Sample Name | Flexural Stress (MPa) | Max. Force (N) | Flexural Strain (%) | Max. Stroke (mm) |
|---|---|---|---|---|
| **1** | 523.00 | 563.75 | 0.85 | 6.88 |
| **2** | 540.65 | 543.91 | 0.88 | 6.94 |
| **3** | 558.42 | 559.22 | 0.88 | 6.97 |
| **4** | 519.59 | 527.81 | 0.93 | 7.26 |
| **5** | 529.05 | 529.38 | 0.85 | 6.56 |
| **Avg.** | **534.14** | **544.81** | **0.87** | **6.92** |
| **St. Dev. (±)** | **14.09** | **14.79** | **0.02** | **0.22** |

As it is known, during the test the force increased continuously up to the maximum value and a sudden failure occurred in the sample. The flexural strength and maximum force of the reference composite samples were calculated as 436.25 MPa and 427.97 N, respectively. It was observed that the addition of PA 66 nanofibers to the junction region resulted in a significant improvement in the flexural strength and modulus of the bonded composites. This result can be attributed to the enhanced bonding capacity between the composite and the adhesive due to the presence of nanofibers in the bonding region. Moreover, the altered matrix properties by interspersing PA66 on the uncured prepreg can improve in-plane bending performance [29,39]. The images of PA66 attached composites after the bending test are shown in Figure 4.14.

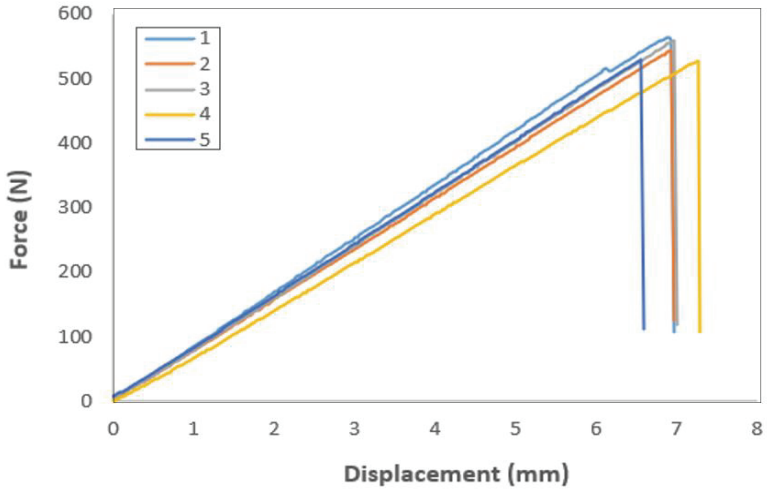


Figure 4. 13. Force vs displacement curve of PA66 added samples under flexural loading.

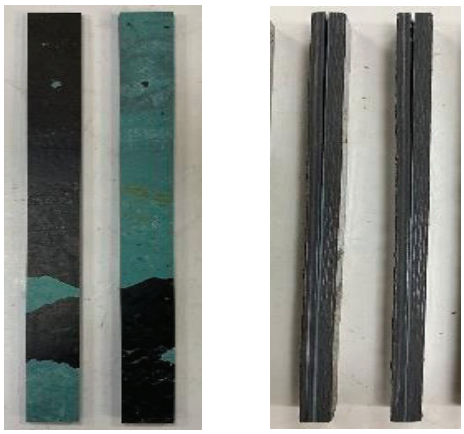

a) b)

Figure 4. 14. Failed a) reference and b) PA66 added composite bending test samples.

Figure 4.15 and Table 4.7 summarize the flexural test results of composite specimens with and without nanofibers. According to the flexural test results, nanofiber materials caused a 22.43% increase in flexural performance of CF/EP composites. Another reason for this increase is that the bending load is distributed between the matrix and the nanofibers act as an energy-absorbing material in the junction region.

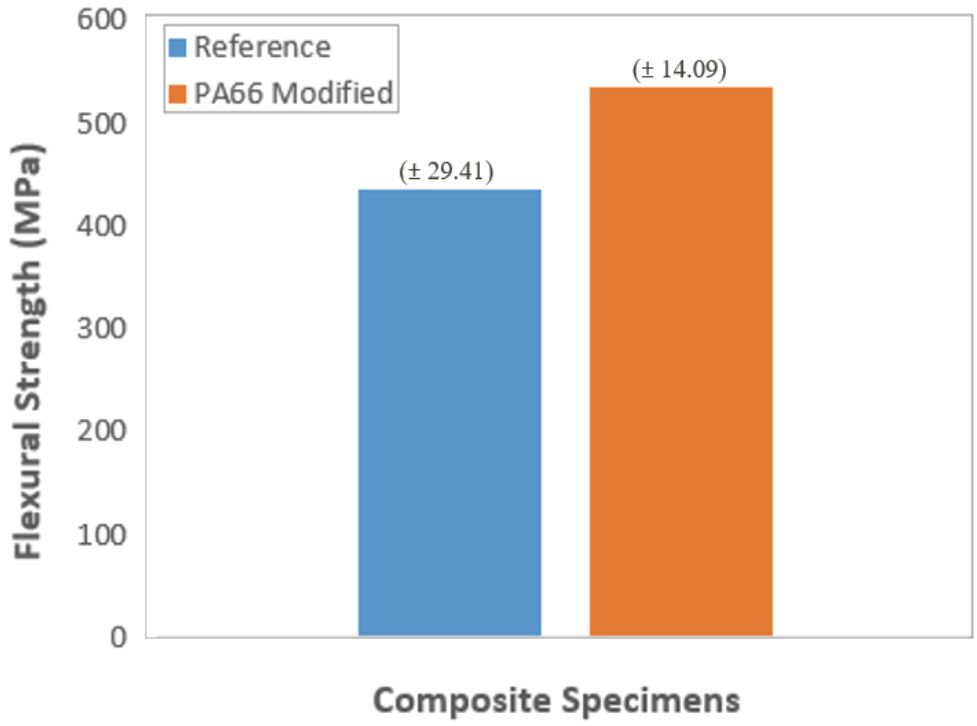


Figure 4. 15. Flexural strength of composite test samples.

Table 4. 7. Summary of Flexural test results.

| Sample Name | Flexural Strength (MPa) | Max. Force (kN) | Flexural Strain (%) |
|---|---|---|---|
| **Reference Avg.** | 436.25 | 428.97 | 0.78 |
| **St. Dev. (±)** | **29.41** | **27.39** | **0.08** |
| **PA66 Modified Avg.** | 534.14 | 544.81 | 0.87 |
| **St. Dev. (±)** | **14.09** | **14.79** | **0.02** |

### 4.3.4. Compression Tests

Compressive properties of materials, especially compressive strength, are one of the most critical factors affecting the design of fiber-reinforced composites. Generally, the tensile strength of a fiber-reinforced composite is higher than the compressive strength. Therefore, compressive strength is considered the weakest link during design. To ensure safer use of the material to be used in engineering applications, it is very important to improve the compressive strength without sacrificing other mechanical properties.

Compression properties of composite samples cured at 180°C and 7 bar pressure and coated with PA66 joint area were investigated. Compression tests were carried out according to ASTM D695-02.

Table 4. 8. Compressive properties of reference samples.

| Sample No | Compressive Strength (MPa) | Elastic Modulus (GPa) | Max. Force (kN) |
|---|---|---|---|
| **R1** | 412.47 | 32.96 | 23.72 |
| **R2** | 428.13 | 32.08 | 26.28 |
| **R3** | 476.04 | 31.59 | 28.69 |
| **R4** | 392.97 | 30.28 | 23.82 |
| **R5** | 414.13 | 30.39 | 24.73 |
| **Avg.** | **424.75** | **31.46** | **25.44** |
| **St. Dev. (±)** | **27.98** | **1.02** | **1.86** |

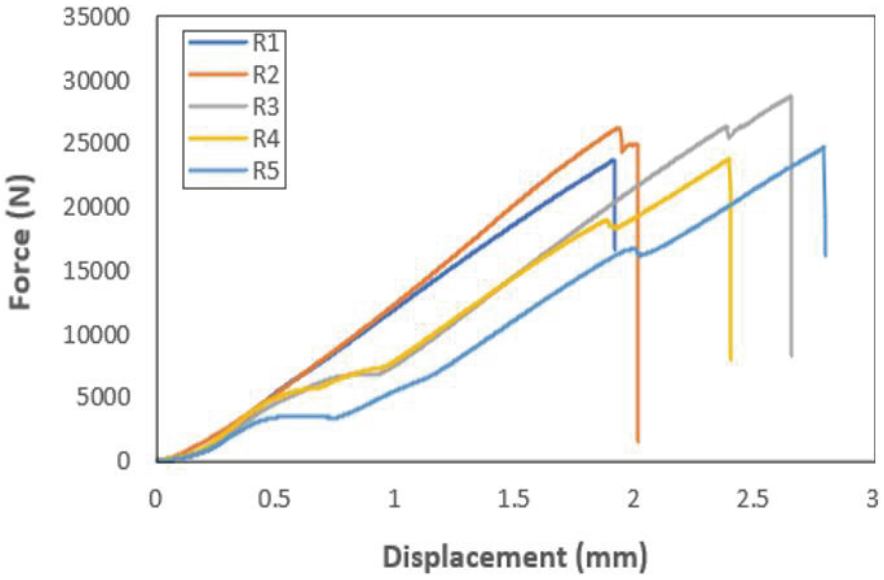


Figure 4. 16. Force vs displacement curve of reference samples under compression loading

The pressure behavior of the reference samples is shown in Figure 4.16. As shown in Table 4.8, the compressive strength and elastic modulus of the reference composites were calculated as 424.75 MPa and 31.46 GPa, respectively. Interspersing PA66 nanofibers at the junctional zone increased the compressive strength of the composites from 424.75 MPa to 490.09 MPa, and the elastic modulus from 31.46 GPa to 38.08 GPa (Table 4.9). The compression behavior of PA66 added samples is given in Figure 4.17. Compressive stress and compressive modulus values were calculated from the force-displacement curve.

Table 4. 9. Compressive properties of P66 added samples.

| **Sample No** | **Compressive Strength (MPa)** | **Elastic Modulus (GPa)** | **Max. Force (kN)** |
|---|---|---|---|
| **1** | 466.34 | 40.67 | 27.46 |
| **2** | 475.92 | 38.47 | 27.88 |
| **3** | 484.62 | 41.31 | 28.43 |
| **4** | 511.92 | 41.60 | 30.45 |
| **5** | 511.67 | 28.35 | 29.70 |
| **Avg.** | **490.09** | **38.08** | **28.78** |
| **St. Dev. (±)** | **18.63** | **4.98** | **1.12** |

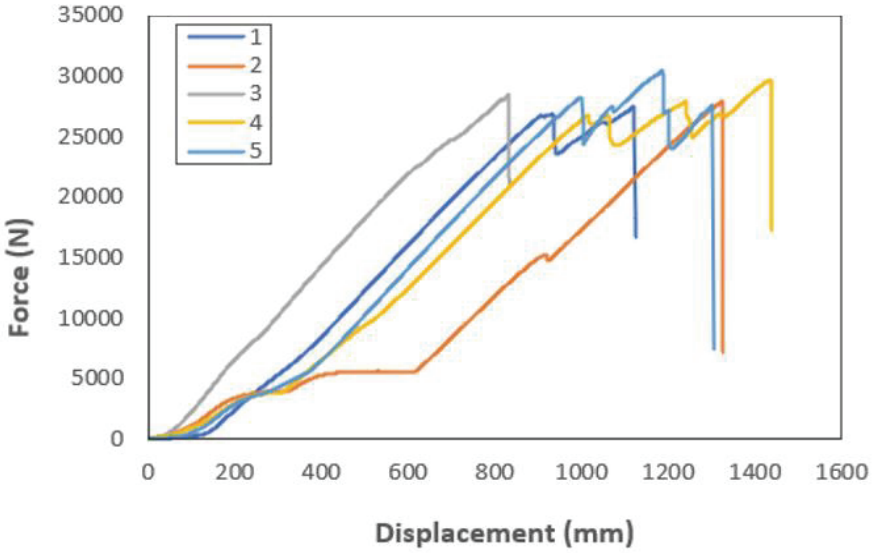


Figure 4.17. Force vs displacement curve of PA66 added samples under compression loading.

Figure 4.18 and Table 4.10 summarize the compression test results of samples with reference and PA66 nanofibers. It was determined that the compressive strength of PA66 composites was higher than that of the reference samples. With the incorporation of PA66 nanofibers, the compressive strength and compressive modulus increased by approximately 15.38% and 21.04%, respectively.

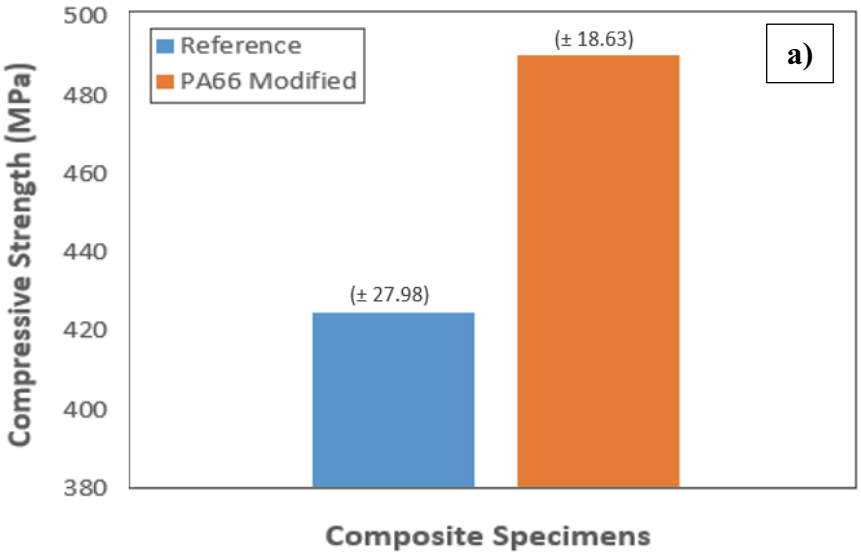


**(cont. on next page)**

Figure 4. 18. a) Compression strength and b) compression modulus of composite test samples.

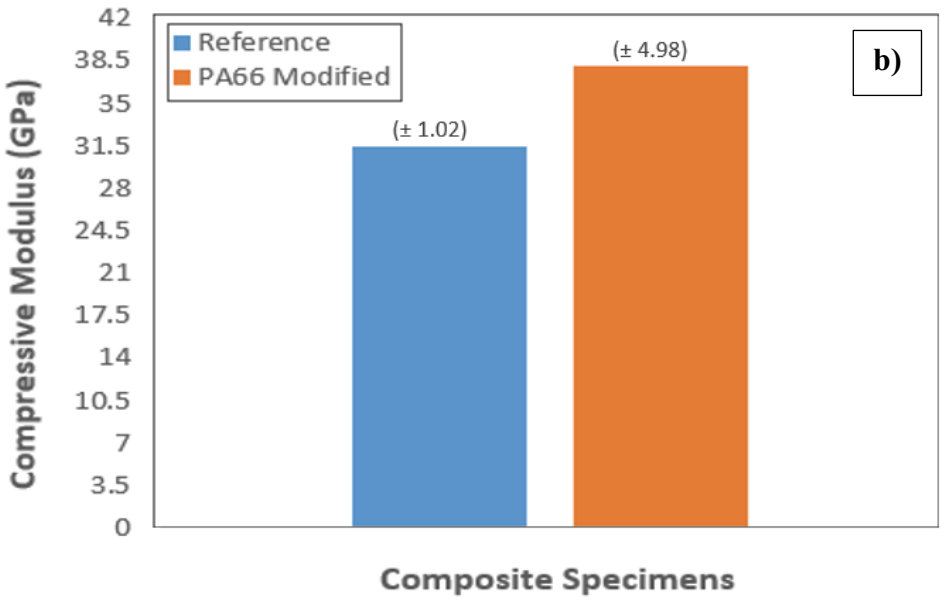


Figure 4.18. (cont.)

Table 4. 10. Summary of compression test results.

| Sample Name | Compressive Strength (MPa) | Elastic Modulus (GPa) | Max. Force (kN) |
|---|---|---|---|
| **Reference Avg.** | 424.75 | 31.46 | 25.44 |
| **St. Dev. (±)** | **27.98** | **1.02** | **1.86** |
| **PA66 Modified Avg.** | 490.09 | 38.08 | 28.78 |
| **St. Dev. (±)** | **18.63** | **4.98** | **1.12** |

SEM images of the reference and PA66 included samples are given in Figure 4.19. It is associated with the matrix material as it provides compressive strength, lateral stiffness and fiber stability in composites. The presence of PA66 nanofibers in the matrix enables the matrix to withstand higher loads in the compressive direction, increasing the compressive strength values of the nanofiber-coated specimens in the joint zone. The nanofibers added to the joint area act as a web and allow the adhesive to adhere better to the fibers. Compared to the reference samples, it was observed that the nanofiber-added composites showed better mechanical bonding performance. These results are supported by the data in the compression test results.

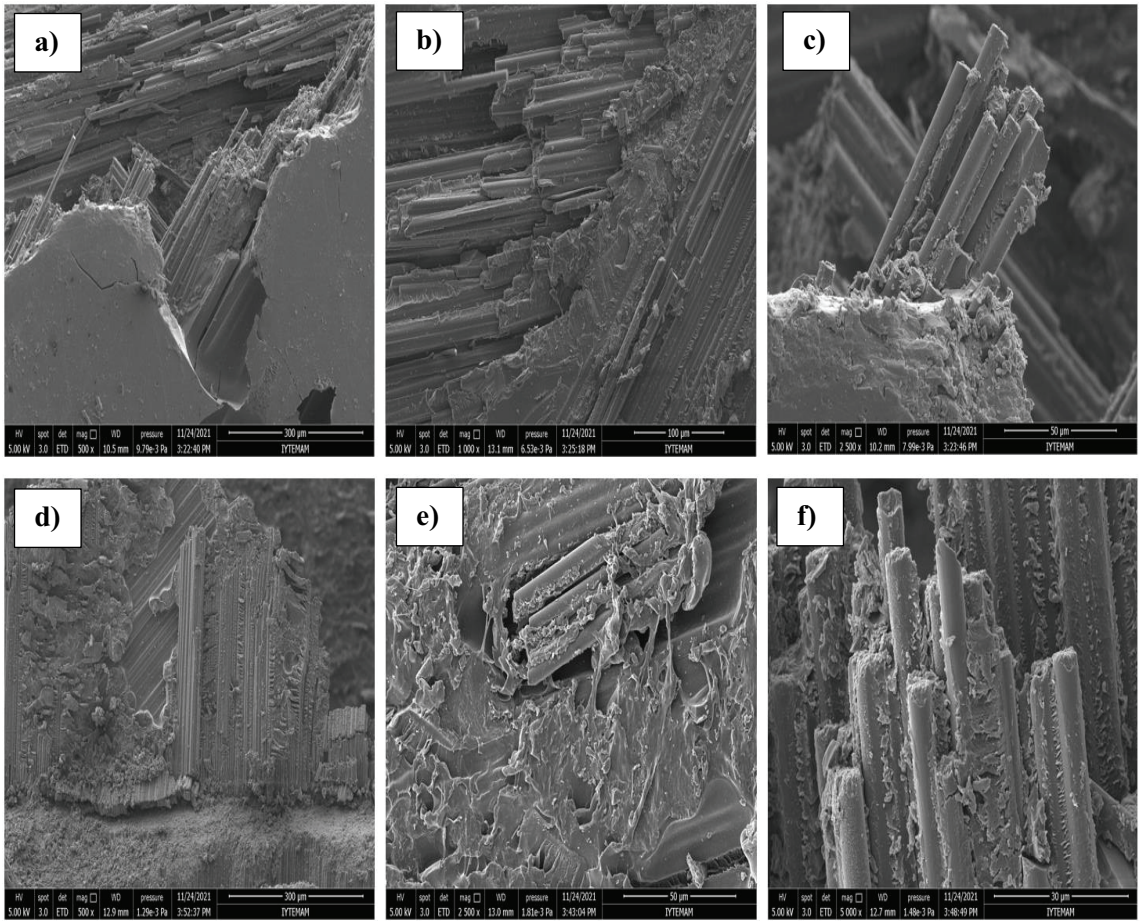


Figure 4. 19. SEM images of the a-b-c) reference and d-e-f) PA66 nanofiber added samples

### 4.3.5. Charpy-Impact Tests

The average Charpy impact energy of the reference samples was measured as 235.68 kJ/m2. SEM images of reference samples are shown in Figure 4.20. In the post-test SEM images, it was observed that the reference samples had a glassy and smooth fracture surface and showed no signs of deformation. These are indicators of weak junctional bond strength and impact energy.

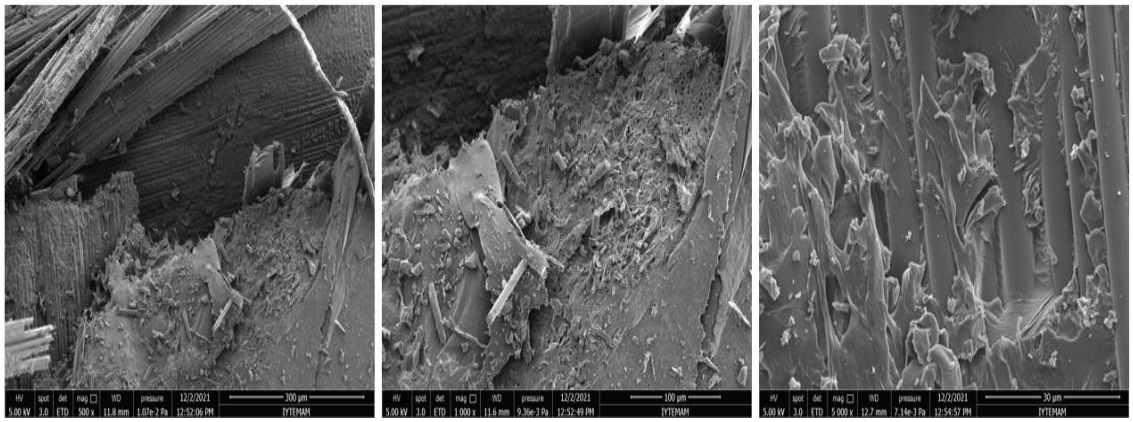

Figure 4. 20. Fracture surface SEM images of reference Charpy-impact specimens

The average Charpy impact energy of the PA66 interspersed composite samples was determined as 596.64 kJ/m2. By adding PA66 nanofibers to the reference composites, the impact energy was increased by approximately 153.15%. Figure 4.21 shows fracture surface SEM images of Charpy-impact test specimens with PA66 added.

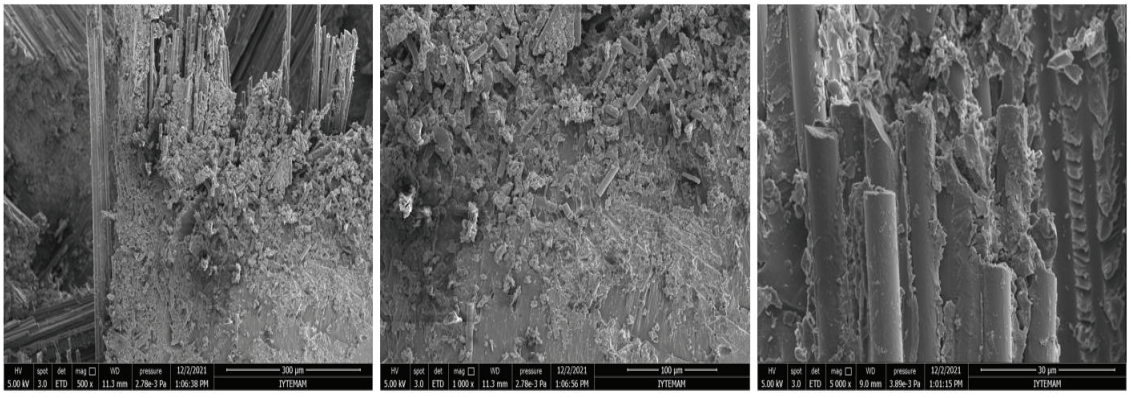

Figure 4. 21. Fracture surface SEM images of PA66 added Charpy-impact specimens

Compared with reference samples, PA66 nanofiber interspersed samples exhibited a more complex and irregular fracture surface in the epoxy matrix, indicating higher plastic deformation and impact energy absorption. Moreover, this improvement is due to the presence of nanofibers between the junctional regions and their contribution to crack resistance at impact, increasing the load-carrying capacity of the samples, and resistance during failure. PA66 nanofibers acted as an energy absorber in the composite.

In addition, when the AWD ratio of nanofibers is increased by a certain amount, it has been proven that the composites absorb a relatively higher amount of energy, which shows higher impact resistance of the composites. Figure 4.22, samples with reference and PA66 added after impact loading.

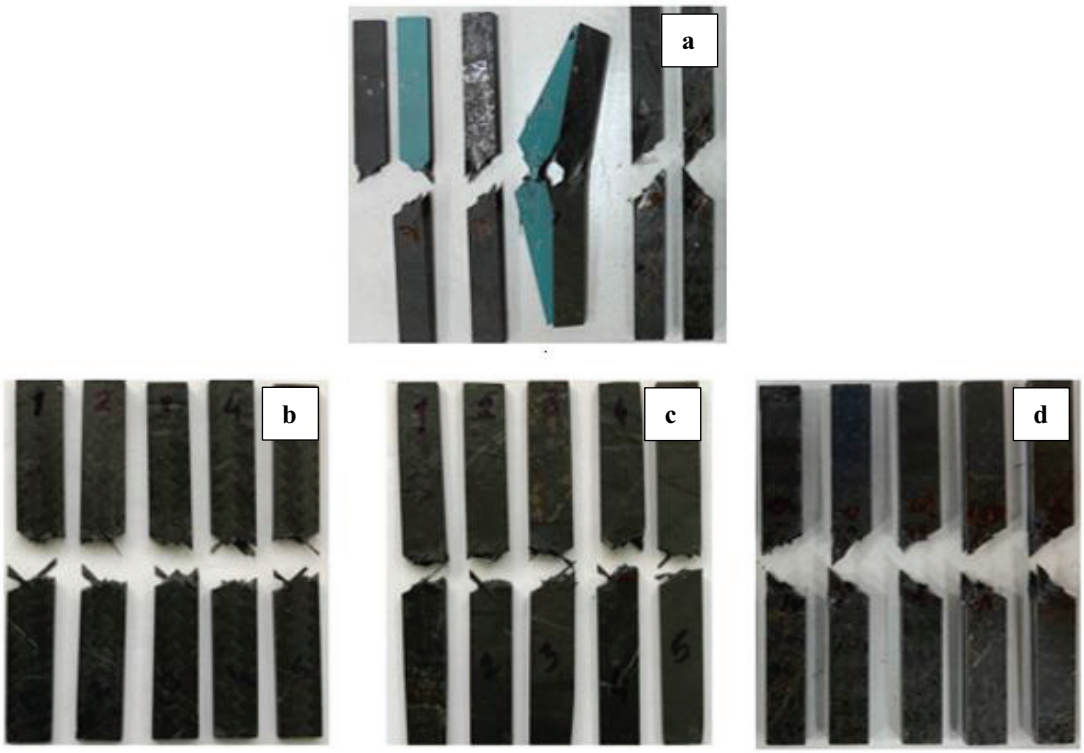


Figure 4. 22. a) Reference, b) Woven, c) UD and d)UD-Woven secondary bonding/PA66 composite test specimens after impact loading.

Table 4. 11. Charpy impact strength of the test specimens.

| Sample | Charpy Impact Strength (kJ/m2) (avg.) | Standard Dev. (±) | Improvement or Reduction (%) |
|---|---|---|---|
| **Reference (Woven)** | 70.85 | 5.70 | - |
| **PA 66 Modified (Woven)** | 78.91 | 8.76 | **+11.37** |
| **Reference (UD)** | 134.97 | 28.16 | - |
| **PA 66 Modified (UD)** | 140.96 | 28.17 | **+4.4** |
| **Reference (Woven/UD-SB)** | 235.68 | 3.03 | - |
| **PA 66 Modified (Woven/UD-SB)** | 596.64 | 5.32 | **+153.15** |

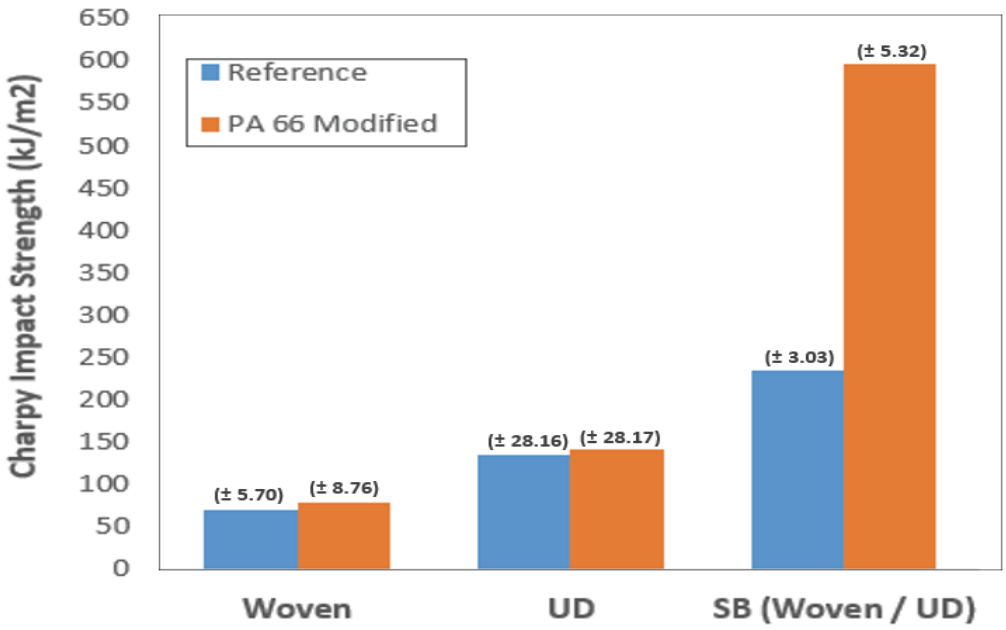


Figure 4. 23. Charpy impact energy of composite test specimens

Figure 4.23 and Table 4.11 show the Charpy impact strength of the test specimens. When the Charpy impact test results were examined, It has been shown that the impact energy of existing CF/EP prepreg plates can be significantly improved using the nanofiber coating method. Compared to the reference samples, the increase in Charpy impact energy was determined as 4.4%, 11.37% and 153.15% for Ud-PA66, woven-PA66 and Ud-woven-PA66-(secondary bonding) composites, respectively. Matrix deformation of the sample and the participation of PA66 nanofibers in impact absorption are the main reasons for this increase in impact energy.

### 4.3.6. Mode-I Fracture Toughness Tests

Figure 4.24 shows the force-displacement plots of the reference samples and PA66 nanofiber-coated DCB samples tested under Mode-I breaking load. The load-displacement curves of the samples were notched as in the reference samples. Maximum load (Fmax) data for reference and PA 66 cured composite samples were calculated as 58.60 N and 71.00 N, respectively.

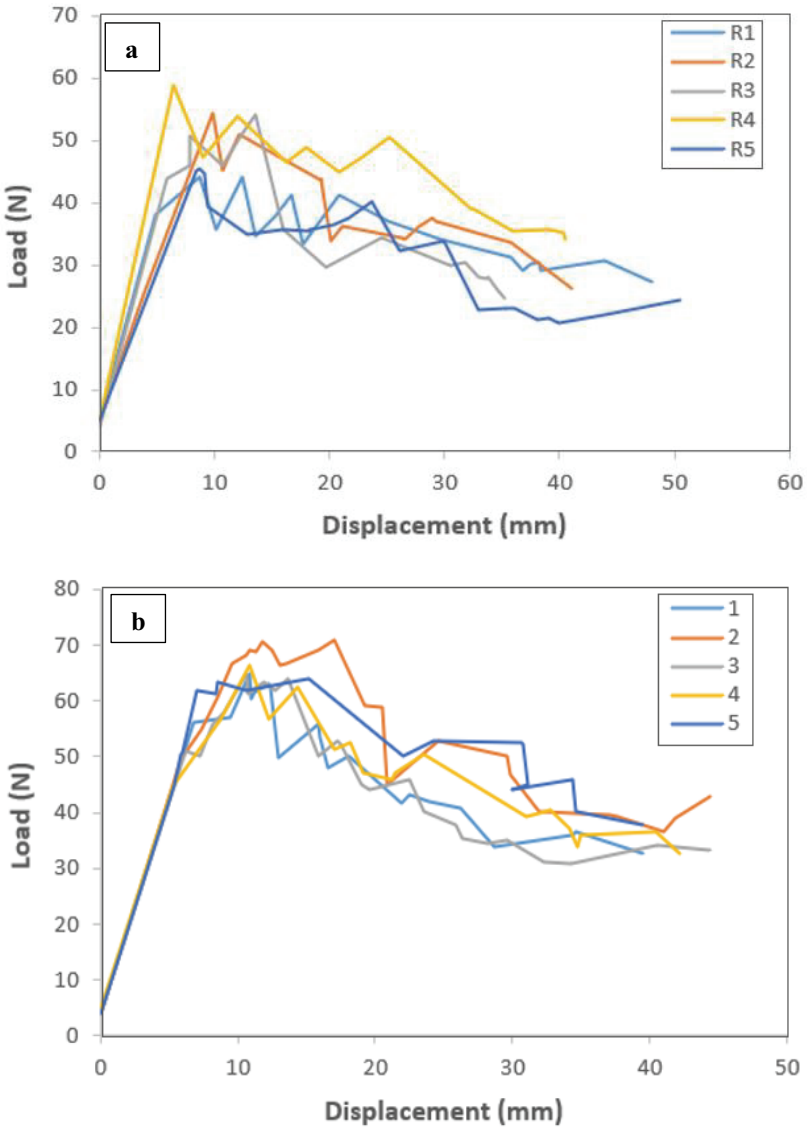


Figure 4. 24. Load-displacement plots of a) reference and b) PA66 added composites under Mode-I loading.

Figure 4.25 shows the $G_{IC}$ and delamination length curve of reference and PA66 added composite samples. The crack initiation and propagation values for the reference samples were calculated as 0.05 and 0.4 J/m2, respectively. The maximum $G_{IC}$ value of the reference composites was determined as 0.77 kJ/m$^2$. Initiation and progression Mod-I fracture toughness values for PA 66 nanofiber interspersed composites were calculated as 0.06 and 0.5 J/m$^2$, respectively. The maximum $G_{IC}$ value of the PA66 modified composites was determined as 0.85 kJ/m$^2$. When the PA66 modified samples were compared with the reference samples, it was determined that the Mod-I fracture toughness value advanced by approximately 10.38%.

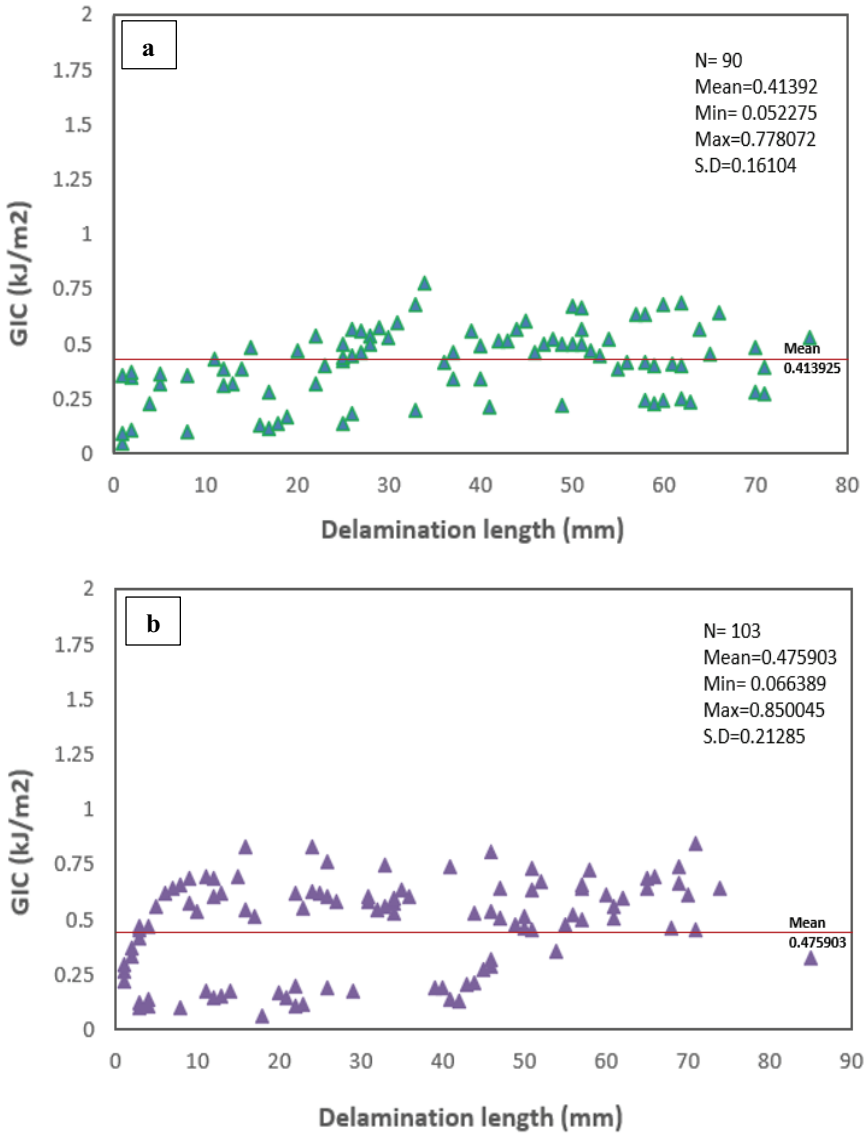


Figure 4. 25. $G_{IC}$ and delamination length curve of a) reference and b) Pa66 added composite samples.

Table 4. 12. Summary of Mod-I fracture toughness test results.

| **Sample Name** | **Mod-I fracture toughness $GIC_{ini}$ (kJ/m²)** | **Mod-I fracture toughness $GIC_{prop}$ (kJ/m²)** | **Max. Mod-I fracture toughness $GIC_{max.}$ (kJ/m²)** | **Max. Force (N)** |
|---|---|---|---|---|
| **Reference Avg.** | 0.05 | 0.4 | 0.77 | 58.60 **(±)4.15** |
| **PA66 Modified Avg.** | 0.06 | 0.5 | 0.85 | 71.00 **(±)1.52** |

Figure 4.26 shows the photograph of DCB surfaces of a PA66 composite after Mode-I testing. Figure 4.27 shows the fracture surfaces of the reference and PA66 interspersed composite samples after DCB testing. Compared with the reference samples, the PA66 coated composite samples showed a different type of fracture behavior. When looking at the reference samples, the separation took place in the adhesion region, while in the PA66 coated composite samples, the separation first started at the adhesive and passed to the woven lamina side. This confirms that the nanofibers increase the adhesive strength of the adhesive.

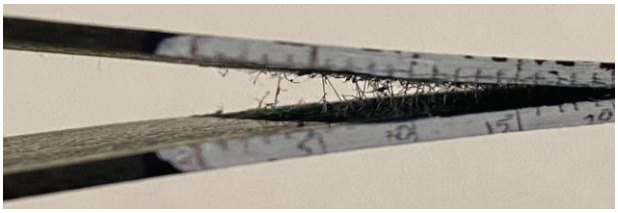

Figure 4. 26. Photographs of PA66 composite specimens under Mode-I loading

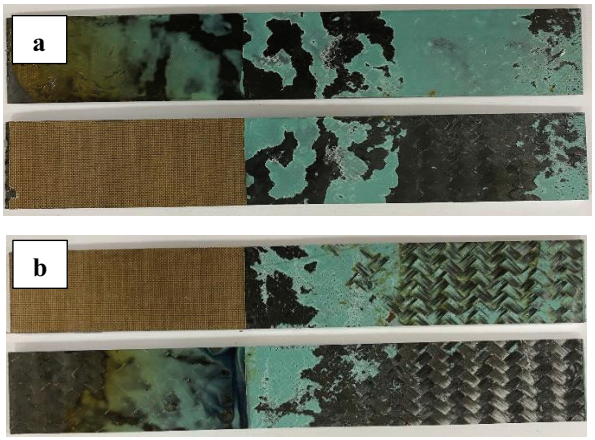


Figure 4. 27. Photograph of the DCB surfaces of fractured a) reference and b) PA66 added composite.

Figure 4.28 shows post-test SEM images of crack surfaces of interspersed PA nanofiber and reference Mod-I samples. Images were taken from the middle part of the crack formation of the samples to interpret the images of the fracture surfaces. During testing, PA66 nanofibers resisted crack propagation in the adhesive with increased Mod I fracture toughness. The fiber bridges formed by the nanofibers held the carbon layers

and adhesive together. PA66 nanofibers created resistance to crack propagation and increased the energy absorption of the composites. The crack had to expend significant energy to separate the PA66 nanofibers. This increased the crack propagation resistance of the composite.

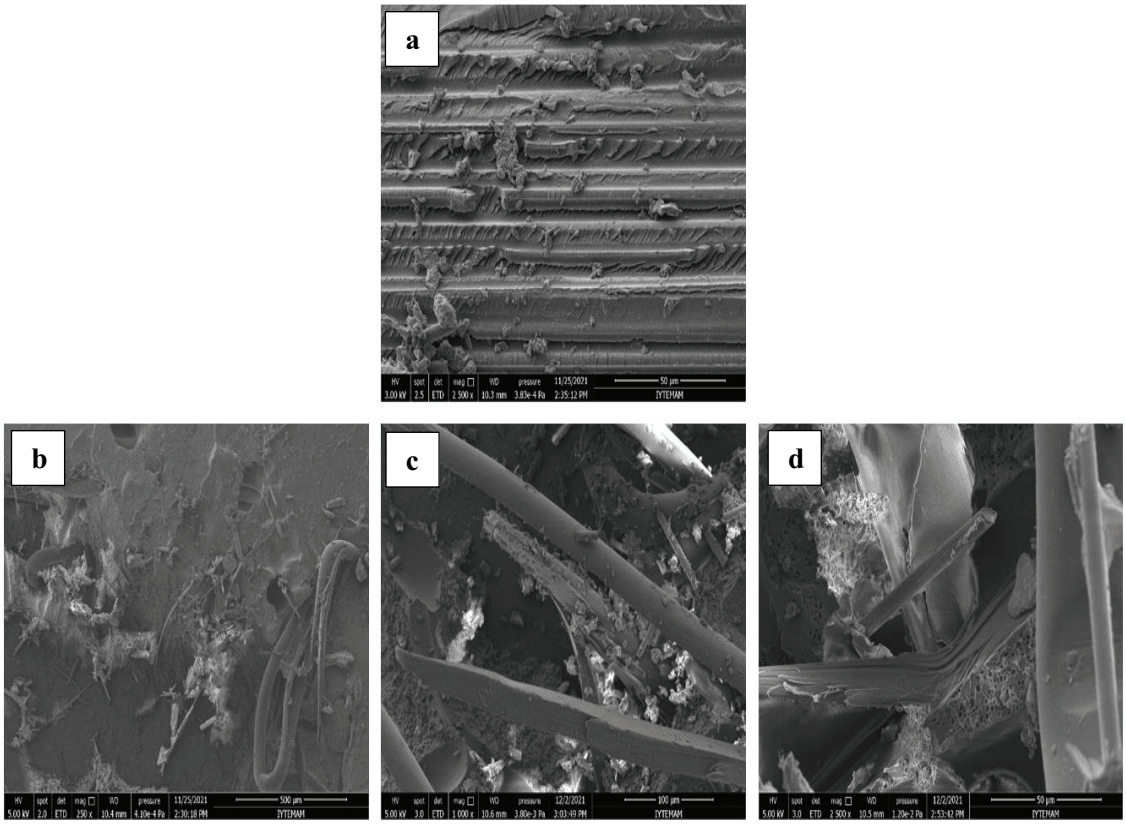


Figure 4. 28. Fracture surface SEM images of a) reference and b-c-d) PA nanofiber interspersed Mode-I reference sample.

Table 4.13 shows the comparison of the mechanical performances of the samples added with PA66 in the joint area with the reference samples, according to the results obtained in this study. This proves that PA 66 nanofiber interleaving by the electro-spinning method is a promising method to improve the joint zone mechanical properties of composites. Table 4.13 shows that the presence of PA 66 nanofibers is effective in improving many mechanical properties of composites such as tensile, compressive, flexural, shear strength and modulus. In general, higher toughness co-occurs with lower strength because there is an inverse relationship between toughness and strength. Improving fracture toughness without sacrificing in-plane mechanical properties makes

the PA66 nanofiber interleaving technique more effective than other techniques in the literature. In addition, it has been proven that the joint zone and in-plane mechanical properties of composites can be improved by using nanofibers at a low AWD ratio. Looking at the literature, it is seen that the average nanofiber diameter obtained in other studies using the PA 66 nanofiber interspersing method is in the range of 85-150 nm.

Table 4. 13. Summarizes the comparison of the mechanical performances of the reference samples and the samples with the addition of PA66.

| Reference | Average nanofiber diameter (nm) | Areal weight density ($g/m^2$) | Nanofiber material | Property | Improvement or reduction (%) |
|---|---|---|---|---|---|
| This study | 36.52± 12 | 1.782 | PA66 | Tensile strength | **+10.17** |
| | | | | Tensile modulus | **+2.61** |
| | | | | Compressive strength | **+15.38** |
| | | | | Compressive modulus | **+21.04** |
| | | | | Flexural strength | **+22.43** |
| | | | | Shear strength | **+18.78** |
| | | | | Charpy impact strength | **+153.15** |
| | | | | Mode-I fracture toughness | **+10.38** |

In this study, the average diameter of the produced nanofibers is 36 nm, and the nanofiber AWD values and coating time are lower than other studies in the literature [29,32,46,47]. Although it is possible to obtain AWD values greater than 2 g/m2 according to other studies, it has been concluded that increasing the nanofiber coating time has a negative effect on the mechanical properties. Electrospinning parameters need to be optimized to observe critical improvements in the mechanical behavior of composites. In addition, it has been determined that nanofibers, which can be produced as homogeneous (beadless structure), play a very important role in achieving higher improvement in the mechanical performance of composites. In addition, the distribution of nanofibers in the junction area can lead to inconsistent results (higher standard deviations) and inaccurate information about the mechanical behavior of composites.

# CHAPTER 5

# CONCLUSIONS

In recent years, the use of composite materials has been increasing in many industrial products, from aircraft parts to bottle caps. Also, prepregs, which reduce the downside of production convenience and excess resin, are becoming practiced more and more preferred in industries. The performance of composite materials can be determined according to parameters such as choosing reinforcement and matrix materials, changing the fiber arrangement and type, or changing the fiber-matrix interface. Today, there has been an increase in demand for higher-performance composite materials in the industry. For this reason, studies are mostly focused on finding ways to improve the mechanical performance of existing composite structures. Nanocomposites, in which nanomaterials (nanofibers, nanoparticles, etc.) are used for reinforcement, offer new solution methods to improve the mechanical properties of composites. The Electro-spinning technique, which is the most effective and easiest method of forming nanofibers, allows us to produce effective materials for reinforcing composites. Nanofibers produced by electrospinning are obtained by interspersing on the uncured prepreg surface or evenly dispersing them into the polymer-based matrix. The addition of nanofibers to composite materials does not cause a significant increase in the thickness of the laminate and the volume fraction of the primary reinforcing fiber.

In this study, it was aimed to improve the joining region mechanical performance of composites by coating PA66 nanofibers to CF/EP prepregs. An innovative joining method has been developed by getting rid of the negative effects (increased weight, stress intensifier, serious delamination problems, corrosion, electromagnetic properties/radar absorption, labor cost and manufacturing process, etc.) of traditionally used mechanical fasteners (screws, rivets, etc.). PA66 nanofibers used for surface improvement were chosen because they are relatively inexpensive, dissolve easily in a wide variety of solvents, have negligible post-coating thickness increase, and have better mechanical properties compared to other polymers. Furthermore, the melting points of PA66 nanofibers are higher than the curing temperature of most composite matrices and they have negligible weight as area weight density. SEM analysis was used to determine

suitable coating parameters (homogeneous and beadless fiber production), investigate the morphology of nanofibers and fracture surfaces of composite samples.

A single lap shear test was applied to demonstrate the effects of PA66 on the bonding zone (adhesion) properties. According to the test results, the shear strength values of the PA66 applied samples improved by 18.78 %. The effect of the optimum thickness of the film adhesive to be used to improve the joint area properties on the sample was investigated. When the 0.4 mm (2 layers) and 0.6 mm (3 layers) thick adhesives applied in shear tests were compared with each other, it was determined that the sample combined with 0.6 mm thick film adhesive showed the best adhesion performance. In line with these results, an 38.27% improvement was achieved in the shear strength values of the samples, which were interspersed with PA66 and adhered with 0.6 mm thick film adhesive. The reasons for the increase in the shear strength of the PA66 added samples are the increase in the surface area, the increase in the surface roughness and therefore the better penetration of the adhesive into the surface. This is because PA66 adheres better to the composite plates and increases the bond strength of the adhesive.

Optimum coating rate, amount of adhesive and spin time were determined according to lap shear test results. When the mechanical test results of the samples coated with these values were examined, it was shown that the use of nanofibers could improve the mechanical properties of the joint zone of the composites. The addition of PA66 nanofibers to the prepregs increased the shear, tensile, compressive and flexural strengths by 18.78%, 10.17%, 15.38% and 22.43%, respectively. Charpy impact energy has also been increased by 153.15%. PA66 nanofibers increased the Mode-I fracture toughness by approximately 10.38 %. Another important observation was the positive effect of nanofibers that increases with increasing the area weight density of nanofibers by a certain amount.

By the fracture surfaces (post-test) of the samples exposed to nanofiber interleaving were examined by SEM, it was observed that the adhesive showed better adhesion properties with the presence of a PA66 layer on the composite surface.

## 5.1. Future Works

- A aging test will be applied to tensile, lap shear, compression and three-point bending specimens.
- The fatigue behavior of added lap-shear specimens will be investigated.
- The mechanical properties of composites will be increased by adding nano-filling materials such as CNT (carbon nanotube) and graphene to PA66 nanofibers.
- Alternatively, the z-pinning method will be used. The prepregs will be joined with fine pins (thin rods/nails with a polymer matrix containing carbon filaments) before bonding and curing.
- Laminate and test coupons will be produced again using the autoclave oven. New data will be obtained.
- To compare the applicability of the data in our study, sample production and analysis combined with mechanical methods (Al-based riveting - fasteners, etc.) will be performed.

# REFERENCES


1. Wulfsberg, J.; Herrmann, A.; Ziegmann, G.; Lonsdorfer, G.; Stöß, N.; Fette, M. Combination of Carbon Fibre Sheet Moulding Compound and Prepreg Compression Moulding in Aerospace Industry. *Procedia Eng.* 2014, *81* (October), 1601–1607. https://doi.org/10.1016/j.proeng.2014.10.197.

2. Cogswell, F. N. The Experience of Thermoplastic Structural Composites during Processing. *Compos. Manuf.* 1991, *2* (3–4), 208–216. https://doi.org/10.1016/0956-7143(91)90142-4.

3. Rangaswamy, H.; M, H. H.; Gowdru Chandrashekarappa, M. P.; Pimenov, D. Y.; Giasin, K.; Wojciechowski, S. Experimental Investigation and Optimization of Compression Moulding Parameters for MWCNT/Glass/Kevlar/Epoxy Composites on Mechanical and Tribological Properties. *J. Mater. Res. Technol.* 2021, *15*, 327–341. https://doi.org/10.1016/j.jmrt.2021.08.037.

4. Davis, G. D. *Surface Treatments of Selected Materials*; 2018; Vol. 1–2. https://doi.org/10.1007/978-3-319-55411-2_8.

5. Turan, K.; Örçen, G. Failure Analysis of Adhesive-Patch-Repaired Edge-Notched Composite Plates. *J. Adhes.* 2017, *93* (4), 328–341. https://doi.org/10.1080/00218464.2015.1116984.

6. Shang, X.; Marques, E. A. S.; Machado, J. J. M.; Carbas, R. J. C.; Jiang, D.; da Silva, L. F. M. Review on Techniques to Improve the Strength of Adhesive Joints with Composite Adherends. *Compos. Part B Eng.* 2019, *177* (August), 107363. https://doi.org/10.1016/j.compositesb.2019.107363.

7. Molitor, P.; Barron, V.; Young, T. Surface Treatment of Titanium for Adhesive Bonding to Polymer Composites: A Review. *Int. J. Adhes. Adhes.* 2001, *21* (2), 129–136. https://doi.org/10.1016/S0143-7496(00)00044-0.

8. Kusano, Y. Atmospheric Pressure Plasma Processing for Polymer Adhesion: A Review. *J. Adhes.* 2014, *90* (9), 755–777. https://doi.org/10.1080/00218464.2013.804407.

9. Brito, C. B. G.; De Cássia Mendonça Sales Contini, R.; Gouvêa, R. F.; De Oliveira, A. S.; Arbelo, M. A.; Donadon, M. V. Mode I Interlaminar Fracture Toughness Analysis of Co-Bonded and Secondary Bonded Carbon Fiber Reinforced Composites Joints. In *Materials Research*; 2017; Vol. 20, pp 873–882. https://doi.org/10.1590/1980-5373-mr-2016-0805.

10. Ma, X.; Yang, Z.; Gu, Y.; Li, Y.; Li, M.; Zhang, D.; Jia, L.; Zhang, Z. Manufacture and Characterization of Carbon Fiber Composite Stiffened Skin by Resin Film Infusion/Prepreg Co-Curing Process. *J. Reinf. Plast. Compos.* 2014, *33* (17), 1559–1573. https://doi.org/10.1177/0731684414543213.

11. Leone, C.; Genna, S. Effects of Surface Laser Treatment on Direct Co-Bonding Strength of CFRP Laminates. *Compos. Struct.* 2018, *194* (March), 240–251. https://doi.org/10.1016/j.compstruct.2018.03.096.

12. Quini, J. G.; Marinucci, G. Polyurethane Structural Adhesives Applied in Automotive Composite Joints. *Mater. Res.* 2012, *15* (3), 434–439. https://doi.org/10.1590/S1516-14392012005000042.

13. Messler. ScienceDirect_articles_14Dec2021_10-51-54. 2004.

14. De Freitas, S. T.; Sinke, J. Adhesion Properties of Bonded Composite-to-Aluminium Joints Using Peel Tests. *J. Adhes.* 2014, *90* (5–6), 511–525. https://doi.org/10.1080/00218464.2013.850424.

15. Zhang, G.; Kataphinan, W.; Teye-Mensah, R.; Katta, P.; Khatri, L.; Evans, E. A.; Chase, G. G.; Ramsier, R. D.; Reneker, D. H. Electrospun Nanofibers for Potential Space-Based Applications. *Mater. Sci. Eng. B Solid-State Mater. Adv. Technol.* 2005, *116* (3 SPEC.ISS.), 353–358. https://doi.org/10.1016/j.mseb.2004.05.050.

16. Lam, H. Le. Electrospinning of Single Wall Carbon Nanotube Reinforced Aligned Fibrils and Yarns. *A Thesis Submitt. to Fac. Drexel Univ.* 2004, *2004* (October), 246.

17. Mohan, A. Formation and Characterization of Electrospun Nonwoven Webs. *Text. Manag. Technol.* 2002.

18. Rostamabadi, H.; Assadpour, E.; Tabarestani, H. S.; Falsafi, S. R.; Jafari, S. M. Electrospinning Approach for Nanoencapsulation of Bioactive Compounds; Recent Advances and Innovations. *Trends in Food Science and Technology*. Elsevier Ltd June 1, 2020, pp 190–209. https://doi.org/10.1016/j.tifs.2020.04.012.

19. Deitzel, J. M.; Kleinmeyer, J.; Harris, D.; Tan, N. C. B. The Effect of Processing Variables on the Morphology of Electrospun Nanofibers and Textiles. *Polymer (Guildf).* 2001.

20. X. Fang; D. H. Reneker. DNA Fibers by Electrospinning X. *J. Macromol. Sci. Part B Phys.* 2006, No. October, 37–41.

21. Larrondo, L.; Manley, R. S. J. Electrostatic Fiber Spinning From Polymer Melts - 3. Electrostatic Deformation of a Pendant Drop of Polymer Melt. *J. Polym. Sci. Part A-2, Polym. Phys.* 1981, *19* (6), 933–940. https://doi.org/10.1002/pol.1981.180190603.

22. Lyons, J.; Li, C.; Ko, F. Melt-Electrospinning Part I: Processing Parameters and Geometric Properties. *Polymer (Guildf).* 2004, *45* (22), 7597–7603. https://doi.org/10.1016/j.polymer.2004.08.071.

23. Kim, C.; Park, S. H.; Lee, W. J.; Yang, K. S. Characteristics of Supercapaitor Electrodes of PBI-Based Carbon Nanofiber Web Prepared by Electrospinning. *Electrochim. Acta* 2004, *50* (2-3 SPEC. ISS.), 877–881.

https://doi.org/10.1016/j.electacta.2004.02.071.

24. Huang, Z. M.; Zhang, Y. Z.; Kotaki, M.; Ramakrishna, S. A Review on Polymer Nanofibers by Electrospinning and Their Applications in Nanocomposites. *Compos. Sci. Technol.* 2003, *63* (15), 2223–2253. https://doi.org/10.1016/S0266-3538(03)00178-7.

25. Lee, K. H.; Kim, H. Y.; Bang, H. J.; Jung, Y. H.; Lee, S. G. The Change of Bead Morphology Formed on Electrospun Polystyrene Fibers. *Polymer (Guildf).* 2003, *44* (14), 4029–4034. https://doi.org/10.1016/S0032-3861(03)00345-8.

26. Uz, Y. C. Development and Characterization of Innovative Fiber Reinforced Prepregs and Their Composites Containing Functional Fillers. 2021.

27. Song, M. G.; Kweon, J. H.; Choi, J. H.; Byun, J. H.; Song, M. H.; Shin, S. J.; Lee, T. J. Effect of Manufacturing Methods on the Shear Strength of Composite Single-Lap Bonded Joints. *Compos. Struct.* 2010, *92* (9), 2194–2202. https://doi.org/10.1016/j.compstruct.2009.08.041.

28. Mohan, J.; Ivanković, A.; Murphy, N. Mixed-Mode Fracture Toughness of Co-Cured and Secondary Bonded Composite Joints. *Eng. Fract. Mech.* 2015, *134*, 148–167. https://doi.org/10.1016/j.engfracmech.2014.12.005.

29. Beylergil, B.; Tanoğlu, M.; Aktaş, E. Enhancement of Interlaminar Fracture Toughness of Carbon Fiber–Epoxy Composites Using Polyamide-6,6 Electrospun Nanofibers. *J. Appl. Polym. Sci.* 2017, *134* (35), 1–12. https://doi.org/10.1002/app.45244.

30. Van der Heijden, S.; Daelemans, L.; Meireman, T.; De Baere, I.; Rahier, H.; Van Paepegem, W.; De Clerck, K. Interlaminar Toughening of Resin Transfer Molded Laminates by Electrospun Polycaprolactone Structures: Effect of the Interleave Morphology. *Compos. Sci. Technol.* 2016, *136*, 10–17. https://doi.org/10.1016/j.compscitech.2016.09.024.

31. Saz-orozco, D.; Ray, D.; Stanley, W. F. Effect of Thermoplastic Veils on Interlaminar Fracture Toughness of a Glass Fiber / Vinyl Ester Composite. 2015. https://doi.org/10.1002/pc.

32. Retolaza, A.; Eguiazábal, J. I.; Nazábal, J. Structure and Mechanical Properties of Polyamide-6,6/Poly(Ethylene Terephthalate) Blends. *Polym. Eng. Sci.* 2004, *44* (8), 1405–1413. https://doi.org/10.1002/pen.20136.

33. Sanatgar, R. H.; Borhani, S.; Ravandi, S. A. H.; Gharehaghaji, A. A. The Influence of Solvent Type and Polymer Concentration on the Physical Properties of Solid State Polymerized PA66 Nanofiber Yarn. *J. Appl. Polym. Sci.* 2012, *126* (3), 1112–1120. https://doi.org/10.1002/app.36871.

34. Beckermann, G. W.; Pickering, K. L. Mode i and Mode II Interlaminar Fracture Toughness of Composite Laminates Interleaved with Electrospun Nanofibre Veils. *Compos. Part A Appl. Sci. Manuf.* 2015, *72*, 11–21.

https://doi.org/10.1016/j.compositesa.2015.01.028.

35. Aljarrah, M. T.; Abdelal, N. R. Improvement of the Mode I Interlaminar Fracture Toughness of Carbon Fiber Composite Reinforced with Electrospun Nylon Nanofiber. *Compos. Part B Eng.* 2019, *165*, 379–385. https://doi.org/10.1016/j.compositesb.2019.01.065.

36. Niu, H.; Wang, X.; Lin, T. Needleless Electrospinning: Influences of Fibre Generator Geometry. *J. Text. Inst.* 2012, *103* (7), 787–794. https://doi.org/10.1080/00405000.2011.608498.

37. Jentzsch, E.; Gül, Ö.; Öznergiz, E. A Comprehensive Electric Field Analysis of a Multifunctional Electrospinning Platform. *J. Electrostat.* 2013, *71* (3), 294–298. https://doi.org/10.1016/j.elstat.2012.12.007.

38. Van der Heijden, S.; Daelemans, L.; De Schoenmaker, B.; De Baere, I.; Rahier, H.; Van Paepegem, W.; De Clerck, K. Interlaminar Toughening of Resin Transfer Moulded Glass Fibre Epoxy Laminates by Polycaprolactone Electrospun Nanofibres. *Compos. Sci. Technol.* 2014, *104*, 66–73. https://doi.org/10.1016/j.compscitech.2014.09.005.

39. Herwan, J.; Al-Bahkali, E.; Khalil, K. A.; Souli, M. Load Bearing Enhancement of Pin Joined Composite Laminates Using Electrospun Polyacrylonitrile Nanofiber Mats. *Arab. J. Chem.* 2016, *9* (2), 262–268. https://doi.org/10.1016/j.arabjc.2015.03.019.

40. Bilge, K.; Venkataraman, S.; Menceloglu, Y. Z.; Papila, M. Global and Local Nanofibrous Interlayer Toughened Composites for Higher In-Plane Strength. *Compos. Part A Appl. Sci. Manuf.* 2014, *58*, 73–76. https://doi.org/10.1016/j.compositesa.2013.12.001.

41. Lee, Y. J.; Ham, S. R.; Kim, J. H.; Yoo, T. H.; Kim, S. R.; Lee, Y. T.; Hwang, D. K.; Angadi, B.; Seo, W. S.; Ju, B. K.; Choi, W. K. Highly Dispersible Buckled Nanospring Carbon Nanotubes for Polymer Nano Composites. *Sci. Rep.* 2018, *8* (1), 1–10. https://doi.org/10.1038/s41598-018-23172-1.

42. Matulevicius, J.; Kliucininkas, L.; Martuzevicius, D.; Krugly, E.; Tichonovas, M.; Baltrusaitis, J. Design and Characterization of Electrospun Polyamide Nanofiber Media for Air Filtration Applications. *J. Nanomater.* 2014, *2014*. https://doi.org/10.1155/2014/859656.

43. ASTM D790. Standard Test Methods for Flexural Properties of Unreinforced and Reinforced Plastics and Electrical Insulating Materials. D790. *Annu. B. ASTM Stand.* 2002, 1–12.

44. Nurashikin, S.; Hazizan, A. Journal of Composite Materials. *J. Compos. Mater.* 2011, *46* (2), 183–191. https://doi.org/10.1106/002199802026980.

45. ASTM D5528-01. Standard Test Method for Mode I Interlaminar Fracture Toughness of Unidirectional Fiber-Reinforced Polymer Matrix Composites. *Am.*

*Stand. Test. Methods* 2014, *03* (Reapproved 2007), 1–12. https://doi.org/10.1520/D5528-13.2.

46. Brugo, T.; Palazzetti, R. The Effect of Thickness of Nylon 6,6 Nanofibrous Mat on Modes I–II Fracture Mechanics of UD and Woven Composite Laminates. *Compos. Struct.* 2016, *154*, 172–178. https://doi.org/10.1016/j.compstruct.2016.07.034.

47. Zhang, S.; Shim, W. S.; Kim, J. Design of Ultra-Fine Nonwovens via Electrospinning of Nylon 6: Spinning Parameters and Filtration Efficiency. *Mater. Des.* 2009, *30* (9), 3659–3666. https://doi.org/10.1016/j.matdes.2009.02.017.